

# Electrical Detection of Singlet Fission in Single Crystal Tetracene Transistors

*Hyuk-Jae Jang,<sup>†,‡,§,\*</sup> Emily G. Bittle,<sup>‡</sup> Qin Zhang,<sup>†,‡</sup> Adam J. Biacchi,<sup>‡</sup> Curt A. Richter,<sup>‡</sup> and  
David J. Gundlach<sup>‡</sup>*

<sup>†</sup>Theiss Research, La Jolla, CA 92037, USA. <sup>‡</sup>Nanoscale Device Characterization Division,  
National Institute of Standards and Technology, 100 Bureau Drive, Gaithersburg, MD 20899,  
USA. <sup>§</sup>Western Digital Corporation, 5601 Great Oaks Parkway, San Jose, CA 95119, USA.

KEYWORDS: single crystalline organic semiconductors, singlet fission, magnetoconductance,  
organic field effect transistors

ABSTRACT: We present the electrical detection of singlet fission in tetracene by using a field-effect transistor (FET). Singlet fission is a photo-induced spin-dependent process, yielding two triplet excitons from the absorption of a single photon. In this study, we engineered a more deterministic platform composed of an organic single crystal FET rather than amorphous or polycrystalline FETs to elucidate spin-dependent processes under magnetic fields. Despite the unipolar operation and relatively high mobility of single crystal tetracene FETs, we were able to manipulate spin dependent processes to detect magnetoconductance (MC) at room temperature

by illuminating the FETs and tuning the bias voltage to adjust majority charge carrier density and trap occupancy. In considering the crystalline direction and magnetic field interactions in tetracene, we show the MC response observed in tetracene FETs to be the result of the singlet fission process.

Understanding and harnessing spin-related phenomena and spin-dependent processes remain a key challenge to realizing applications for organic semiconductor based device technology.<sup>1-4</sup> Spin-dependent processes play a crucial role in determining and enhancing the efficiency of organic-based devices such as organic light emitting diodes (OLEDs) and organic photovoltaics (OPVs).<sup>3-7</sup> Among the most widely used methods for studying spin-dependent processes in organic-based devices is the application of an externally applied magnetic field.<sup>3,4, 7-11</sup> An applied external magnetic field is known to perturb the ratio of singlet and triplet excited states, resulting in changes of the electronic and optoelectronic properties of the organic-based devices such as electrical resistance and electroluminescence.<sup>3,4</sup> However, the physical mechanisms behind spin-dependent processes controlling (opto-) electronic properties under magnetic fields remain a topic of scientific debate.<sup>4</sup> This is partly due to the experimental studies conducted to date which have largely been based on devices or test structures made from amorphous or polycrystalline thin films of organic semiconductors.<sup>4</sup> Previous studies have favored structurally disordered organic systems because it was suggested that more charge carrier trap sites and longer time between charge carrier hops (consistent with a low charge carrier mobility) enhance the aforementioned magnetic field effects by providing polaron pairs with enough time to interact with the local random hyperfine fields present in organic semiconductors.<sup>12</sup>

Intrigued by the lack of consensus on the theories describing the phenomena observed in thin film based organic devices, we engineered device test structures with a higher degree of structural order by using organic single crystals. The better-defined crystallographic directions and transport pathways provide a test platform which may be more deterministic for elucidating spin-dependent processes under magnetic fields. Specifically, we investigated unipolar (hole transport) field effect transistors (FETs) made from single crystals of tetracene. Tetracene, a widely studied small molecule organic semiconductor, is particularly interesting because it is known to exhibit an uncommon spin-dependent process: singlet fission.<sup>9, 13-18</sup> Unlike intersystem crossing of a two-charge carrier system induced by either hyperfine interaction or spin-orbit coupling which creates a triplet from a singlet exciton by reversing the spin of one charge carrier,<sup>4</sup> singlet fission involves four charge carriers of two molecules, thus generating two triplets from a singlet without requiring any spin reversal.<sup>19-22</sup> We found that our single crystal tetracene FETs produced not only a typical monotonic change of electrical resistance under magnetic fields when illuminated, but also peculiar features not previously reported on in detail. By considering the crystal orientation of tetracene and related dipolar and Zeeman interactions, we show that the features are byproducts of singlet fission/triplet fusion processes. In addition, in the process of elucidating the spin-dependent processes related to singlet fission, we engineered a device structure to achieve a few percent of magnetoresistance in our photoactive field-effect transistors at room temperature, which can contribute to the development of technology of multi-functional electronic devices such as light-controlled FET/ magnetic field sensor.<sup>23, 24</sup>

## **RESULTS AND DISCUSSION**

The device structure of our single crystal tetracene FETs is illustrated in the inset of Figure 1a along with electrical and magnetic field measurement configurations (see Experimental Methods section). Plotted in Figure 1a is the electrical characteristics of a tetracene FET fabricated with Cytop gate dielectric (see Methods section) measured under broadband illumination and in the dark. The FETs display p-type conduction behavior, *i.e.* the majority charge carriers are holes. When the FETs are illuminated, an increase in drain current ( $I_D$ ) is observed; especially, in the sub-threshold (low gate bias,  $V_{GS}$ ) regime. Previous reports suggested the photo-enhanced current can be produced by charge carriers generated at illuminated electrodes as well as in the bulk of the tetracene crystal.<sup>25</sup> The contribution of the bulk crystal to photocurrent has been attributed to the creation of triplet excitons in tetracene *via* the singlet fission process  $S_0 + S_1 \rightarrow T_1 + T_1$ . Where  $S_0$  represents the singlet ground state and  $S_1$  and  $T_1$  represent the first excited singlet and triplet state, respectively.<sup>26-28</sup> The increase in the population of triplet excitons is believed to facilitate the de-trapping of localized charge carriers *via* the process  $T_1 + n^* \rightarrow S_0 + n$ . Triplet excitons can also dissociate into secondary charge carriers as the result of their interaction with trapped (or free) charge carriers as described by the process  $T_1 + n (n^*) \rightarrow e + h + n (n^*)$ , where  $n (n^*)$ ,  $e$ , and  $h$  represent a free (trapped) charge carrier, an electron, and a hole.<sup>28</sup>

The magnetic field dependence of  $I_D$  was measured by applying an external in-plane magnetic field as depicted in the inset of Figure 1a. Plotted in the inset to Figure 1b is the measured magnetoconductance (MC) of a tetracene FET fabricated with Cytop gate dielectric in the dark and under a broadband illumination intensity of  $34 \text{ mW/cm}^2$ . The FET has a channel length of  $50 \text{ }\mu\text{m}$  and was biased with constant gate-source ( $V_{GS}$ ) and drain-source ( $V_{DS}$ ) voltages. MC is defined as  $[I_D(B) - I_D(B = 0)] / I_D(B = 0)$  where  $B$  is the magnitude of the applied magnetic field.

The external magnetic field was swept between -230 mT and 230 mT. For our tetracene FETs measured under illumination, we found that the magnitude of the  $I_D$  ( $|I_D|$ ) decreased with increasing external magnetic field; showing a negative MC response. When measured in the dark, no change in the  $I_D$  was measured with an applied magnetic field, as expected for our FETs which exhibit unipolar operation and have a higher mobility ( $\geq 0.2 \text{ cm}^2 \text{ V}^{-1} \text{ s}^{-1}$ , see Supporting Information) than most thin film based devices.<sup>4, 12</sup> The change in the  $I_D$  with magnetic field when illuminated is attributed to the creation of electron-hole pairs and minority charge carriers.<sup>4</sup>

Although a broad band light source was used for the experiments described here, we were able to define the approximate spectral response of the observed MC by using filters (see Supporting Information). We found that the spectral range of  $\approx 350 \text{ nm}$  to  $\approx 615 \text{ nm}$  produces MC in our single crystalline tetracene FETs. The spectral range agrees with that of previous reports of photocurrent in a magnetic field<sup>29</sup> for tetracene, as well as, the ground-state light absorption spectrum of tetracene.<sup>30, 31</sup> Because the photocurrent is related to the creation of triplet excitons in tetracene *via* the singlet fission process, a negative MC is consistent with the reduction of photo-generated triplet population under magnetic fields.<sup>28</sup> This is likely caused by the splitting of triplet energy levels by Zeeman effect.<sup>4, 7, 27</sup>

Plotted in Figure 1b is the magnitude of the MC ( $|MC|$ ) at  $\approx 200 \text{ mT}$  *versus*  $V_{GS}$  measured in the dark and under illumination. We found a large drop in the  $|MC|$  followed by saturation as the magnitude of  $V_{GS}$  ( $|V_{GS}|$ ) increased above the threshold voltage of the device. As  $|V_{GS}|$  increases,  $|I_D|$  is expected to increase because the charge carrier density increases in the conducting channel as a result of the Fermi level in tetracene shifting towards the mobility edge. With increasing  $|V_{GS}|$ , in gap donor states (traps) are emptied and the rate of triplet exciton quenching by trapped charges

diminishes. Our data imply that triplet exciton quenching by trapped charge has a significant effect on MC in tetracene FETs.

Despite the observation of MC in organic FETs (OFETs) fabricated with Cytop gate dielectric, further studies on magnetic-field dependent phenomena in single crystalline tetracene were limited due to low MC signals. However, by changing dielectric interface to the silicon dioxide ( $\text{SiO}_2$ ) we are able to alter the interface trap density and enhance our MC signal without introducing grain boundaries or disorder in the tetracene crystal (see Figure S2). Plotted in Figure 2a is the electrical characteristics of a single crystal tetracene FETs fabricated with  $\text{SiO}_2$  gate dielectric and measured under illumination and in the dark. Similar to tetracene FETs fabricated with Cytop gate dielectric, the FETs fabricated with  $\text{SiO}_2$  gate dielectric display p-type conduction behavior and an increase in drain current with illumination, especially in the sub threshold regime (at low  $V_{\text{GS}}$ ). The magnetic field dependence of  $I_{\text{D}}$  in FETs prepared on  $\text{SiO}_2$  gate dielectric was measured and showed a  $10 \times$  increase in MC signal under illumination compared to FETs prepared on Cytop gate dielectric, see Figure 2b. Cytop dielectric provided better charge carrier transport/mobility characteristics, but  $\text{SiO}_2$  dielectric offered superior MC effects. No change in the  $I_{\text{D}}$  with an external magnetic field was observed when measured in the dark, consistent with the previous observations for FETs fabricated with Cytop gate dielectric.

The inset to Figure 3a shows the measured MC measured in the dark and under an illumination intensity of  $21 \text{ mW/cm}^2$  of a tetracene FET fabricated with  $\text{SiO}_2$  gate dielectric. The FET had a channel length of  $10 \text{ }\mu\text{m}$ . The measured  $|\text{MC}|$  and  $|I_{\text{D}}|$  at  $200 \text{ mT}$  *versus* the illumination intensity are plotted in Figure 3a. The data show that both  $|\text{MC}|$  and  $|I_{\text{D}}|$  become larger as the illumination intensity increases. In addition to the illumination intensity, we found that by changing  $V_{\text{GS}}$  we can tune the  $|\text{MC}|$  of the single crystalline tetracene FETs fabricated with  $\text{SiO}_2$  gate dielectric even

more effectively than for the FETs fabricated with Cytop gate dielectric, see Figure 3b. A large drop in the  $|MC|$  was observed as the magnitude of  $V_{GS}$  ( $|V_{GS}|$ ) increased in the subthreshold region, from 0 V to 10 V. For  $|V_{GS}|$  greater than the threshold voltage ( $V_{th} \approx 5$  V), the  $|MC|$  reaches a saturation value at around 0.5 %. This is likely because shallow donor (trap) sites are emptied as discussed earlier.

This freedom in using  $V_{GS}$  to tune MC allowed us to maximize the MC signal while minimizing noise for electrically probing the changes induced by magnetic field dependent processes in an organic semiconductor. Figure 2b and the inset to Figure 3 show the MC dependence on magnetic field strength. Interestingly, we observe a photo-induced MC feature around 42 mT not previously reported on for MC studies of a thin film based tetracene FETs.<sup>27</sup>

Previous luminescence and fluorescence spectroscopy studies suggested that singlet fission/triplet fusion processes ( $S_0 + S_1 \leftrightarrow T_1 + T_1$ ) are reversible and they are main sources of magnetic field dependent behavior in tetracene crystals.<sup>28</sup> It was suggested that a magnetic field dependence of singlet fission/triplet fusion processes is due to an interplay between the Zeeman effect and intramolecular magnetic (electron spin) dipolar interaction. Given this, we should then expect to observe a dependence of MC on the direction of the applied magnetic field with respect to the crystallographic axes of the tetracene crystal.<sup>26</sup>

Crystallographic directional dependence of magnetic field effects in the systems with singlet fission was demonstrated in high magnetic field regime (higher than 300 mT) where only two triplet pair states have singlet character, thus being involved in the triplet fusion process. Consequently, the observed anisotropic magnetic field effects were attributed to the level crossing resonance of these two states occurring at a certain crystallographic orientation.<sup>26</sup> A theoretical model based on the Zeeman effect and the magnetic dipolar interaction of triplet excitons in a

tetracene crystal predicts a crystallographic directional dependence of magnetic field effects due to the energy level crossing also at lower magnetic fields (less than 100 mT). Under an applied external magnetic field, a spin Hamiltonian,  $H$  of triplet excitons in molecular crystals can be described by the following equation:<sup>32</sup>

$$H = g\mu_B \mathbf{B} \cdot \mathbf{S} + D^* \left[ S_z^2 - \frac{S(S+1)}{3} \right] + E^* [S_x^2 - S_y^2] \quad (1)$$

where  $g$  is the electron  $g$  factor,  $\mu_B$  is the Bohr magneton,  $\mathbf{B}$  is an external magnetic field,  $\mathbf{S}$  is the spin operator of an electron of the triplet in units of  $\hbar$  (reduced Planck constant), and  $D^*$  and  $E^*$  are molecular parameters provided by the electron paramagnetic resonance (EPR) measurements.<sup>33</sup> The first term in the equation (1) describes the Zeeman effect and the remaining two terms represent the energy induced by the magnetic dipole-dipole interaction between two electrons in a triplet exciton. The magnetic dipolar interaction is also referred to as zero-field splitting since it lifts the degeneracy of the three triplet states even in the absence of external magnetic fields.<sup>10</sup> The Hamiltonian  $H$  can be calculated by using Pauli matrices for the system with spin 1. For the values of  $D^*$  and  $E^*$  of tetracene crystals,  $-0.0062 \text{ cm}^{-1}$  and  $0.0248 \text{ cm}^{-1}$ , respectively were obtained in the previous electron paramagnetic resonance (EPR) measurements.<sup>33</sup> The diagonalization of the  $H$  produces the three eigenvalues ( $E_x$ ,  $E_y$ , and  $E_z$ ) and eigenstates ( $|x\rangle$ ,  $|y\rangle$ , and  $|z\rangle$ ) for a triplet exciton. For two correlated, but non-interacting triplet excitons, the nine triplet pair states can be described as a combination ( $E_{\alpha\beta} = E_\alpha + E_\beta$  for the energy and  $|\alpha\beta\rangle = |\alpha\rangle|\beta\rangle$  for the spin state, where  $\alpha$  and  $\beta$  are either  $x$ ,  $y$ , or  $z$ ).<sup>33, 34</sup>

For a tetracene crystal, the molecular  $x$ - and  $z$ -axes are known to be located in the crystal  $a$ - and  $b$ - axes plane of the crystal,<sup>10, 33, 34</sup> which typically corresponds to the largest natural facet of platelet-like crystals.<sup>35</sup> The tetracene crystals used in this study are platelet-like and subsequently placed on the prefabricated device substrate as a final process step in fabricating the FET test

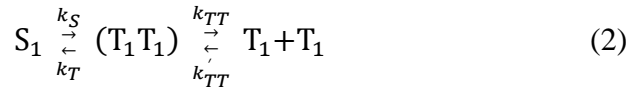
structures. Thus, in our investigation of singlet fission under an in-plane magnetic field, only two molecular axes,  $x$ - and  $z$ -axes, need to be examined for the theoretical consideration. In addition, because the nine triplet pair states created by singlet fission are coupled to the initially excited singlet state, only five triplet pair states having a singlet character ( $|xx\rangle$ ,  $|yy\rangle$ ,  $|zz\rangle$ ,  $|yz\rangle$ , and  $|zy\rangle$  for the applied magnetic field along the  $x$ -axis and  $|xx\rangle$ ,  $|yy\rangle$ ,  $|zz\rangle$ ,  $|xy\rangle$ , and  $|yx\rangle$  along the  $z$ -axis).<sup>10, 34</sup> Figure 4a and 4b illustrate the magnetic field dependence of calculated energies of these five triplet pair states when the magnetic field is applied along  $x$ -axis and  $z$ -axis, respectively. As shown in Figure 4a, paired triplet energy states experience an energy level crossing around the magnitude of 42 mT of an external magnetic field applied along the  $x$ -axis. However, this energy level crossing disappears when the magnetic field is rotated to the  $z$ -axis as shown in Figure 4b.

We carried out angular dependent MC measurements on our tetracene FETs to determine if the features near  $\pm 42$  mT we observe in the measured MC response of our tetracene FETs under illumination is due to a change in triplet population *via* triplet sub-energy level crossing as predicted by the theoretical framework presented in the prior section. Specifically, the FET was rotated relative to the in plane magnetic field axis, as described in the top of Figure 5. The feature around 42 mT in the MC response only appeared when the transistor was aligned with the external magnetic field at a specific angle (near  $\theta = 0^\circ$ ) and disappeared as the device was rotated away from that angle as illustrated in Figure 5.

The  $\theta$  in Figure 5 describes the clockwise rotational angle of the transistor from the original position where the sample axis crossing two electrodes are perpendicular to the applied magnetic field axis. We attribute the shoulder in the  $|MC|$  at  $\approx 42$  mT when the  $x$ -axis of the crystal is parallel to the magnetic field direction to the weakening of the magnetic field effects by the degeneracy in triplet pair states as are result of energy level crossing in intermediate paired triplet states created

by singlet fission. We note the presence of an additional feature between  $\pm 10$  mT in the measured MC response, see Figure 5. As the magnitude of an external magnetic field increases from 0 mT, we observe evidence of weak positive MC before transitioning to negative MC, thus producing a small dip around 0 mT. This weak field positive MC feature is present in the MC response for all measured  $\theta$ s, but its width is narrower about  $\theta = 0^\circ$  than  $\theta = 90^\circ$ .

To better confirm whether the shoulder features near 42 mT and the weak field positive MC feature are the products of singlet fission/triplet fusion processes, we performed a numerical simulation of the MC by adopting a model proposed by Timmel *et al.*<sup>36,37</sup> The excited singlet state responsible for generating nine intermediate triplet pair states in singlet fission process,  $|S^1\rangle$  can be described as a superposition of pair product of two triplet states,<sup>10</sup> and thus  $|S^1\rangle = (1/\sqrt{3})(|x_0\rangle|x_0\rangle + |y_0\rangle|y_0\rangle + |z_0\rangle|z_0\rangle)$  where  $|x_0\rangle$ ,  $|y_0\rangle$ , and  $|z_0\rangle$  are the eigenstates of the Hamiltonian described in equation (1) when  $B = 0$ . In general, the singlet fission/triplet fusion processes can be described as



where  $(T_1 T_1)$  represents the intermediate triplet pair states, and  $k_S$ ,  $k_T$ ,  $k_{TT}$ , and  $k'_{TT}$  are the rate constants for each process.<sup>10</sup> For our calculation, we considered only the processes involved with  $k_S$  and  $k_T$  since they are the magnetic field dependent processes.<sup>10</sup> Based on the Liouville-von Neumann equation, the coherent evolution of the excited spin states under the influence of a spin Hamiltonian can be calculated. Assuming the singlet fission rate constant  $k_S$  is equal to the triplet fusion rate constant  $k_T$  ( $k_S = k_T = k$ ), the steady state yield of excited triplet and singlet states under a magnetic field  $B$ ,  $\Phi_T(B)$  and  $\Phi_S(B)$  can be expressed as follows:<sup>36</sup>

$$\Phi_S(B) = 1 - \Phi_T(B) = \sum_{m=1}^M \sum_{n=1}^M |P_{mn}^S|^2 f(\omega_{mn}) \quad (3)$$

where  $f(x) = \frac{k^2}{k^2+x^2}$ ,  $\omega_{mn} = \frac{E_m-E_n}{\hbar}$ ,  $P_{mn}^S = \langle n|\hat{P}^S|m\rangle$ ,  $\hat{P}^S = |S^1\rangle\langle S^1|$ , and  $M$  is the total number of triplet pair states (in our case,  $M=9$ ). Furthermore, assuming the steady state triplet pairs created by singlet fission evolve into two triplets contributing to the electrical current, but steady state singlets produced by triplet fusion recombine, MC is described as

$$\text{MC}(\text{B}) = \frac{\Phi_{\text{T}}(\text{B}) - \Phi_{\text{T}}(0)}{\Phi_{\text{T}}(0)} \quad (4)$$

with  $\Phi_{\text{T}}(\text{B})$  given by equation (3). Figure 6a and 6b show the simulated MC using equations (3) and (4) as a function of a magnetic field applied along  $x$ - and  $z$ - axes, respectively. For our calculations, we used  $1.0$  (nsec<sup>-1</sup>) for  $k$ .<sup>10</sup> The calculated MC data suggest that both the dip and the humps can be attributed to singlet fission/triplet fusion processes. When a magnetic field is applied along  $x$ -axis, a dip around  $0$  mT and humps around  $42$  mT in MC are produced due to sub-energy level crossings in paired triplet states. However, the humps disappear and the width of the dip widens as the magnetic field is rotated and applied along  $z$ -axis.

Our simulated curves based on a simplified analytical model capture the salient features of the experimental MC data from single crystalline tetracene FETs in a framework grounded in the physics of magnetic field dependent singlet fission/triplet fusion processes. Details not accurately captured by the simplified model, such as the relative magnitudes of the features around  $42$  mT and the depth of the dip in calculated MC, are likely to be better captured by using sophisticated models that incorporate more robust rate constants and account for all the magnetic field dependent processes present in the system. For example, a previous study suggested that Wannier-type excited spin states can also be created by absorbing photons along with triplet pair states through singlet fission, and thus the intersystem crossing between Wannier-type triplets and singlets by random hyperfine fields can occur and their relative population can be disturbed by magnetic fields.<sup>29</sup> It has been reported that the MC due to the intersystem crossing caused by random

hyperfine fields in organic semiconductor based systems can be well fit with either Lorentzian ( $B^2/(B_0^2+B^2)$ ) or non-Lorentzian ( $B^2/(B_0+|B|)^2$ ) equations.<sup>4, 7</sup> If one adds this empirical non-Lorentzian (or Lorentzian) to our simulated MC curves considering that the Wannier-type excited spin states also contributes to the MC, one may improve the similarity between the simulated and the measured MC response (see Supporting Information).

## CONCLUSION

we experimentally demonstrated that a single crystal organic field effect transistor can be used as a more deterministic platform to elucidate the underlying physics of spin-dependent process under magnetic fields than thin film based systems. By using single crystal tetracene FETs, we demonstrate the ability to electrically detect singlet fission/triplet fusion processes under illumination at room temperature along with previously unreported features in the measured magnetoconductance. By considering the nature of singlet fission/triplet fusion processes and magnetic interactions present in tetracene single crystals, we show the unusual features in MC to originate from triplet sub-energy level crossing under magnetic fields through their related angular dependence on the applied magnetic field. Our findings provide a platform to elucidate the fundamental mechanisms of spin-dependent processes such as singlet fission in organic semiconductors and they also furnish a way in the development of multifunctional magneto-optoelectronic applications.

## EXPERIMENTAL METHODS

**Preparation of devices.** The FETs were made on two different test beds: Cytop and SiO<sub>2</sub> gate dielectric. One test bed (Cytop) has a bilayer gate dielectric consisting of a 300 nm thick spin

coated Cytop (Amorphous Fluoropolymer) layer on top of a 50 nm thick silicon dioxide layer which was thermally grown on a heavily doped silicon substrate (n-type  $10^{-3} \Omega \text{ cm}$ ) and photolithographically defined metal electrodes made of 30 nm thick palladium on 5 nm thick titanium. The other test bed ( $\text{SiO}_2$ ) is composed of a single 200 nm thick thermally grown silicon dioxide layer as a gate dielectric and photolithographically defined metal electrodes made of 40 nm thick platinum on 2 nm thick titanium. Tetracene single crystals were grown by physical vapor transport in a tube oven under argon flow. The crystals were carefully laminated to the surface of the test beds, completing the FET fabrication process. Thickness of crystals used for the study are on the order of 0.7 microns, and the light absorption through the crystals should be approximately the same. The two photolithographically defined metal electrodes were biased as the source and drain contact of the FET. The heavily doped silicon substrate was contacted from the wafer back side to form gate contact. The single crystal tetracene FETs had channel lengths that ranged from 5  $\mu\text{m}$  to 100  $\mu\text{m}$ . A self-assembled monolayer of octadecyltrichlorosilane was used to improve the semiconductor adhesion and create a hydrophobic surface on the  $\text{SiO}_2$  that limits adsorbed water at the FET channel interface for the test beds with a single  $\text{SiO}_2$  gate dielectric layer.<sup>38,39</sup>

**Electrical measurements.** Electrical and magnetic field measurements were carried out at room temperature in a commercially available probe station with an attached electromagnet. The measurements were performed under a nitrogen gas environment to minimize possible device degradation and hysteresis in the electrical characteristics. The devices were illuminated by a commercial fiber optic illuminator and through the glass window of the probe station. The illumination intensity was measured with a commercial silicon photodiode. Our fiber optic illuminator has a spectrum of wavelengths that range from  $\approx 350 \text{ nm}$  to  $\approx 1400 \text{ nm}$ , and thus it is expected to allow the light only in that range of wavelengths to reach the devices. During magnetic

field measurements and with applied constant bias voltages, we observed some linear drift in the measured current and corrected for tilt when plotting magnetoconductance.

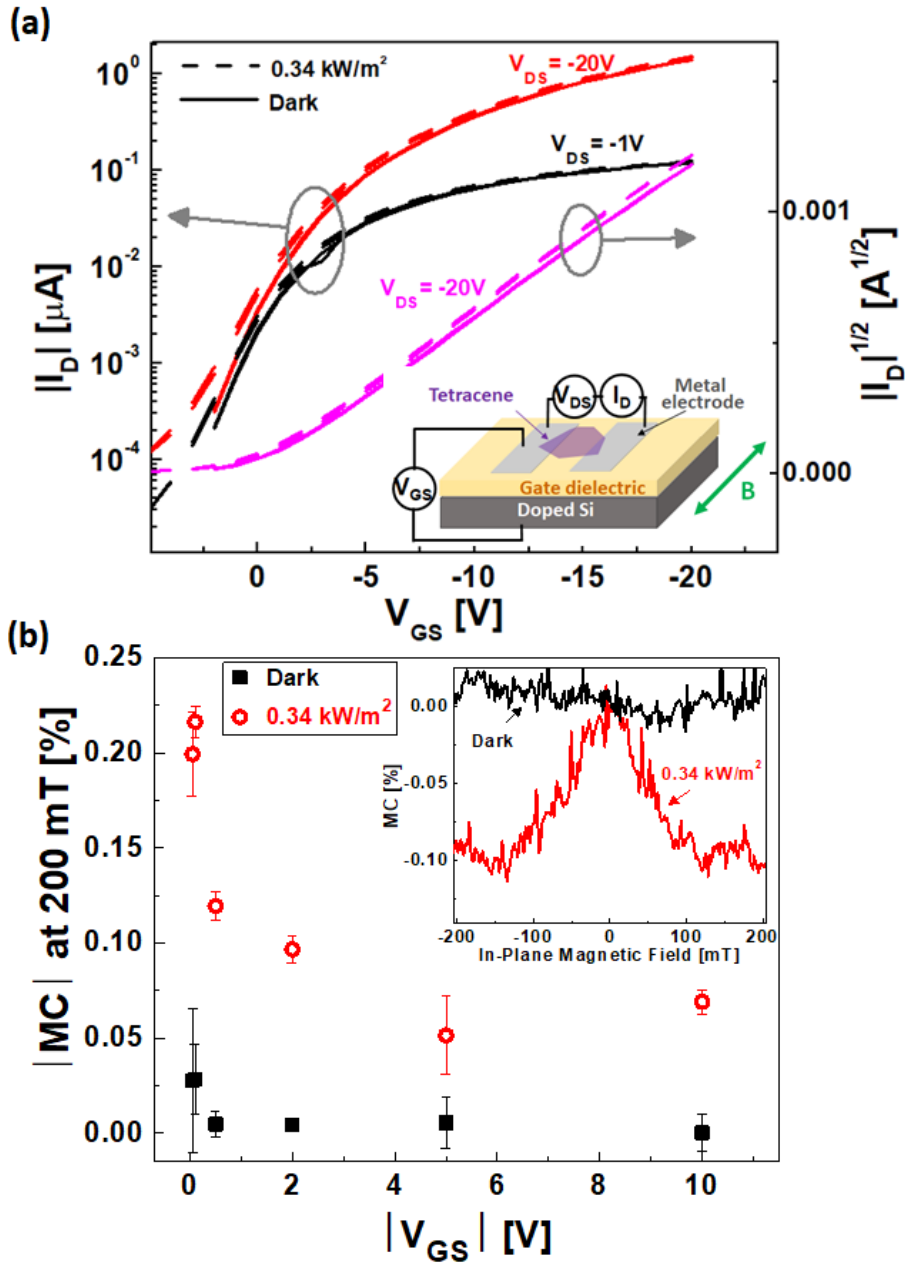
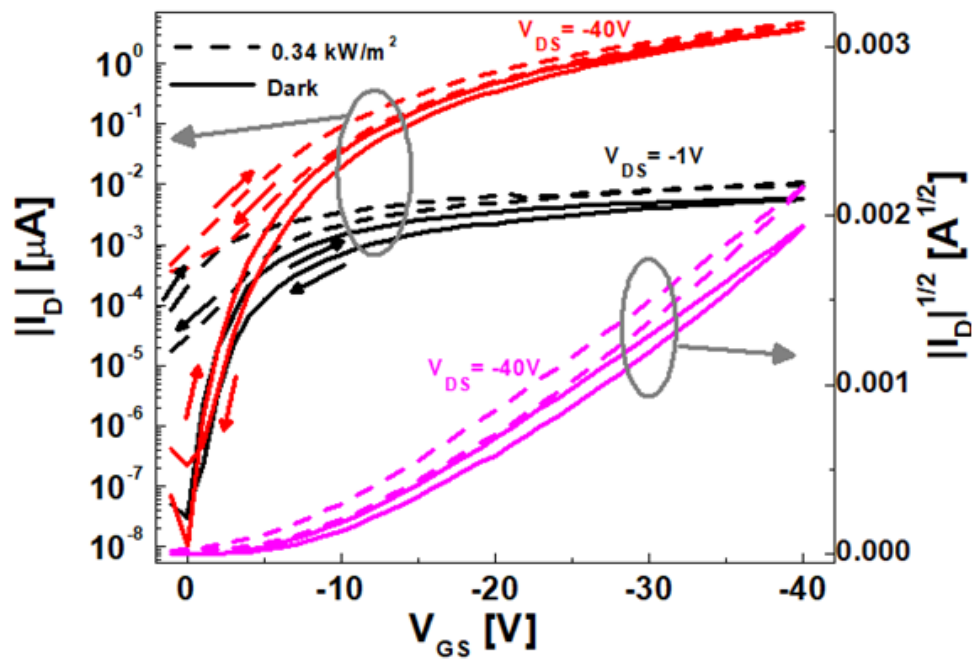


Figure 1

**Figure 1.** Device structure and electrical characteristics of a single crystal tetracene FET fabricated with Cytop gate dielectric. (a) Magnitude of drain current,  $|I_D|$  versus gate-source voltage ( $V_{GS}$ ) of a single crystal tetracene FET (Cytop gate dielectric) measured at a drain-source voltage ( $V_{DS}$ ) of -1 V (black lines) and -20 V (red lines), and square root of  $I_D$  versus  $V_{GS}$  at  $V_{DS} = -20$  V (saturation regime) (magenta lines). Dark measurements are indicated by solid lines; measurements made under illumination are indicated by dashed lines. Inset: schematic view of a single crystal tetracene FET and illustration of the electrical and the magnetic field measurement setups. (b) Magnitude of magnetoconductance ( $|MC|$ ) at a magnetic field of approximately 200 mT versus the magnitude of  $V_{GS}$  measured in the dark (black filled squares) and under illumination (red open circles),  $|V_{GS}|$ . Inset: MC measured by sweeping an external magnetic field between 230 mT and -230 mT measured under illumination (red line) and in the dark (black line) for  $V_{DS} = -1$  V and  $V_{GS} = -2$  V.

(a)



(b)

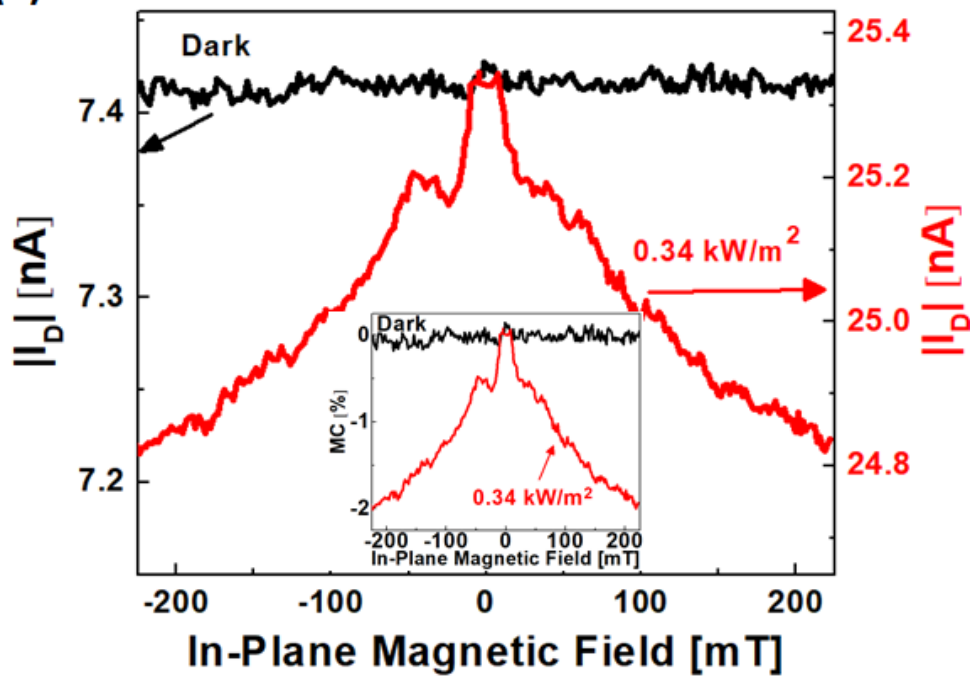


Figure 2

**Figure 2.** Electrical characteristics of a single crystal tetracene FET fabricated with SiO<sub>2</sub> gate dielectric. (a) Magnitude of drain current ( $|I_D|$ ) *versus* gate-source bias ( $V_{GS}$ ) of a single crystal tetracene FET (SiO<sub>2</sub> gate dielectric) measured at a drain-source voltage ( $V_{DS}$ ) of -1 V (black lines) and -40 V (red lines), and square root of  $I_D$  *versus*  $V_{GS}$  at  $V_{DS} = -40$  V (saturation regime) (magenta lines) in the dark (solid lines) and under illumination (dashed lines). Hysteresis in  $|I_D|$  is evidence for charge trapping: for the forward sweep direction ( $V_{GS}$  from 0 V to -40 V),  $|I_D|$  is higher than that for the reverse sweep ( $V_{GS}$  from -40 V to 0 V) for all measurements. (b) Change in  $|I_D|$  measured by sweeping the external magnetic field between 230 mT and -230 mT under illumination (red line) and in the dark (black line) for  $V_{DS} = -20$  V and  $V_{GS} = -2.5$  V.

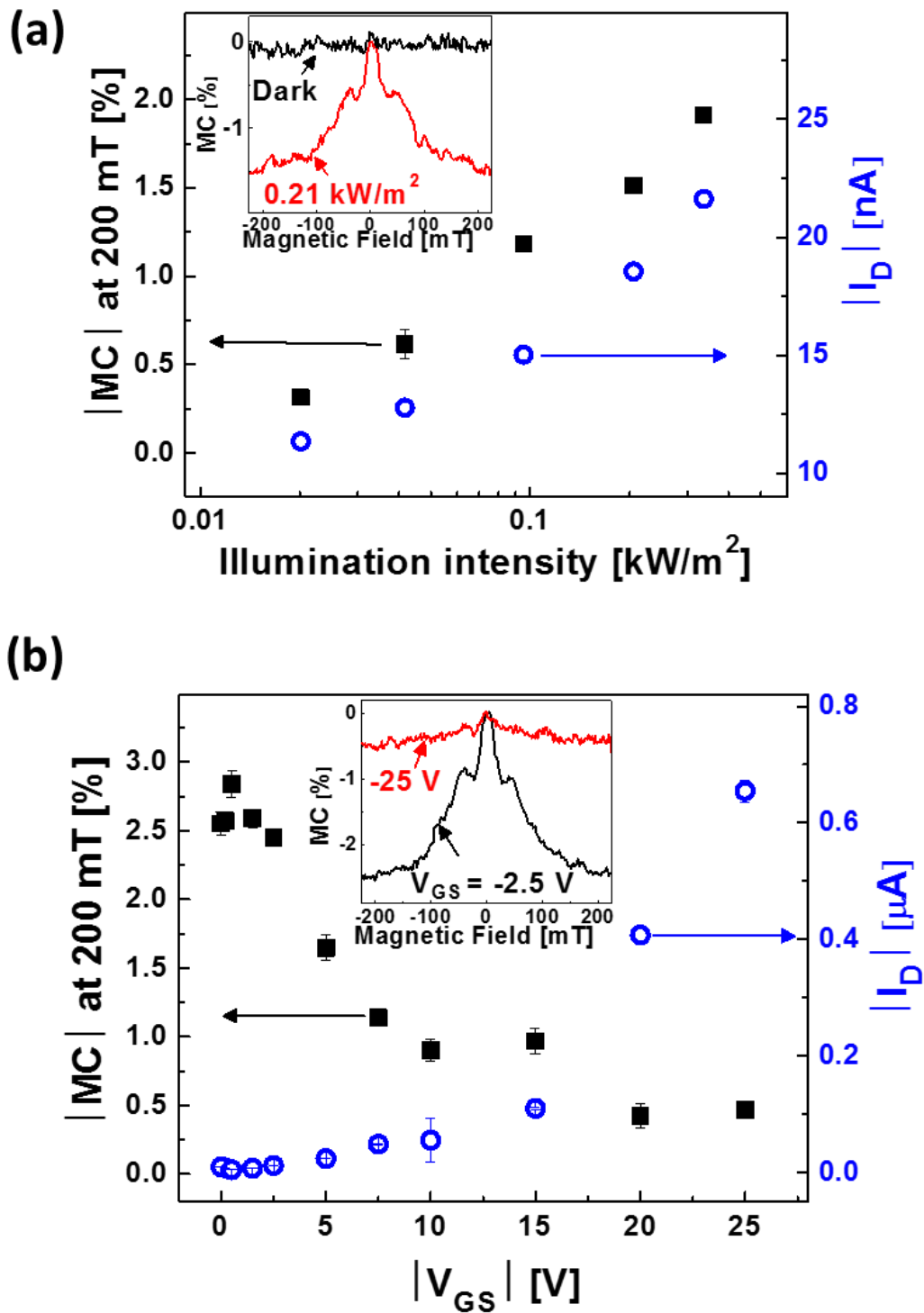


Figure 3

**Figure 3.** Magnetoconductance and drain current of a single crystal tetracene FET fabricated with SiO<sub>2</sub> gate dielectric. Magnitude of magnetoconductance ( $|MC|$ ) measured at a magnetic field of approximately 200 mT (black filled squares) and the magnitude of I<sub>D</sub> ( $|I_D|$ ) (blue open circles) *versus* (a) illumination intensity and (b) the magnitude of V<sub>GS</sub> ( $|V_{GS}|$ ). Inset to figure 3a: MC measured under illumination (red line) and in the dark (black line) with V<sub>DS</sub> = -20 V and V<sub>GS</sub> = -2.5 V. Inset to figure 3b: MC measured with V<sub>GS</sub> = -2.5 V (black line) and -25 V (red line) under the illumination and with V<sub>DS</sub> = -20 V.  $|MC|$  and  $|I_D|$  in the plot are the mean of the values of  $|MC|$  and  $|I_D|$ , respectively at -200 mT and 200 mT. Error bars give the standard deviation of the mean.

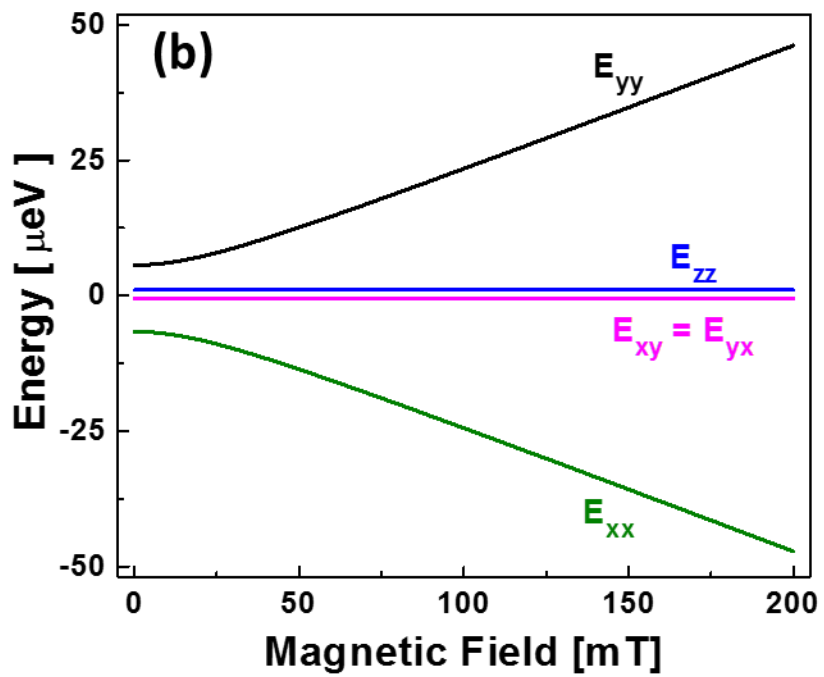
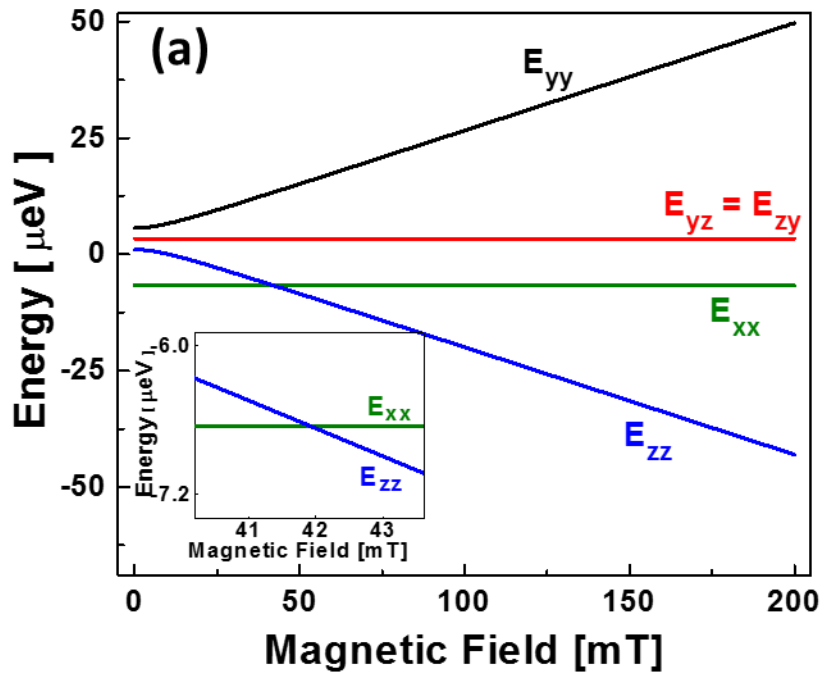


Figure 4

**Figure 4.** Calculated magnetic field dependence of triplet pair state energy. Magnetic field dependence of triplet pair state energies (for pair states having a singlet character) when the magnetic field is applied along the (a)  $x$ -axis and (b)  $z$ -axis directions. Inset to (a): Calculated triplet pair state energy *versus* magnetic field plotted for a narrower range around the level crossing point at approximately 42 mT.

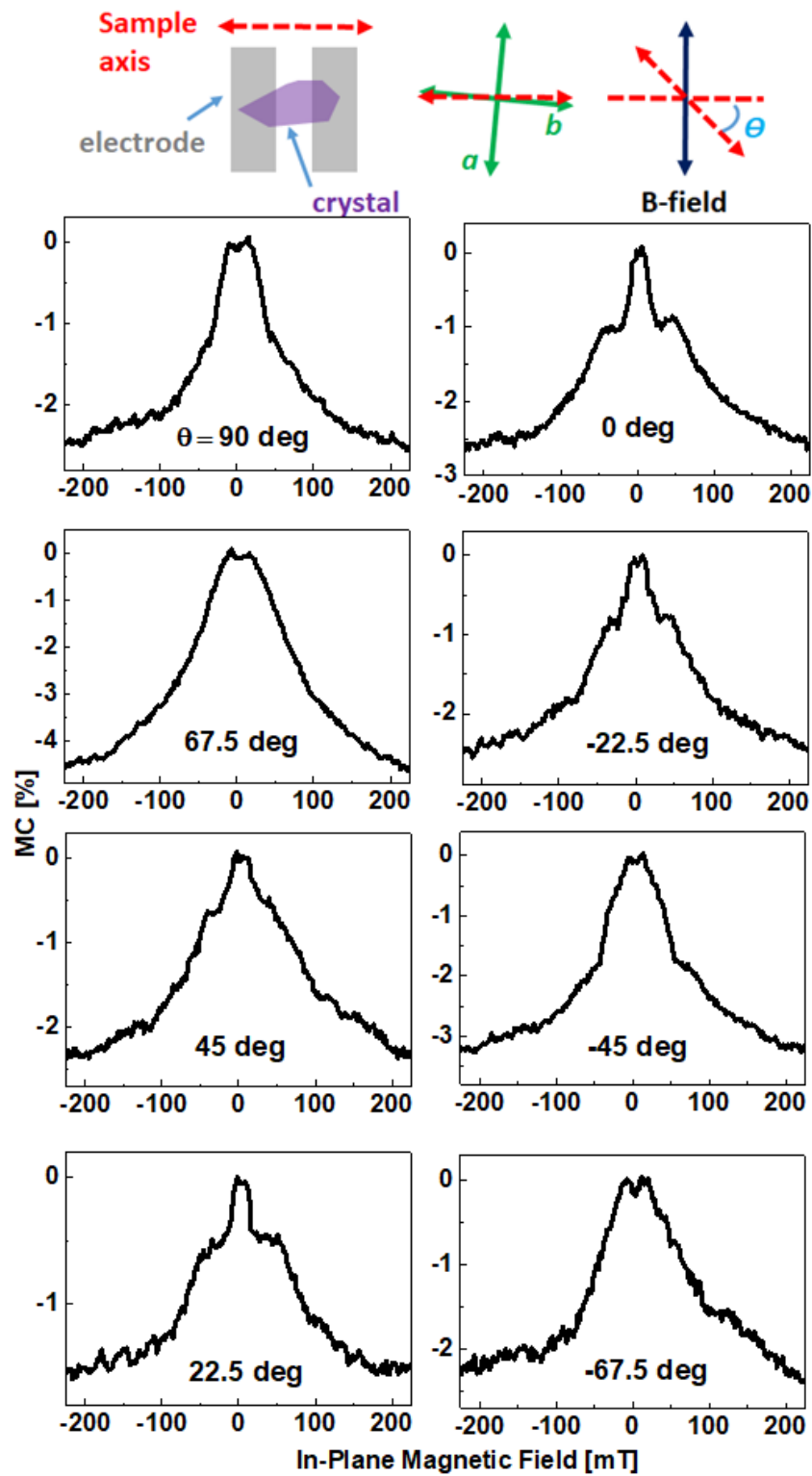
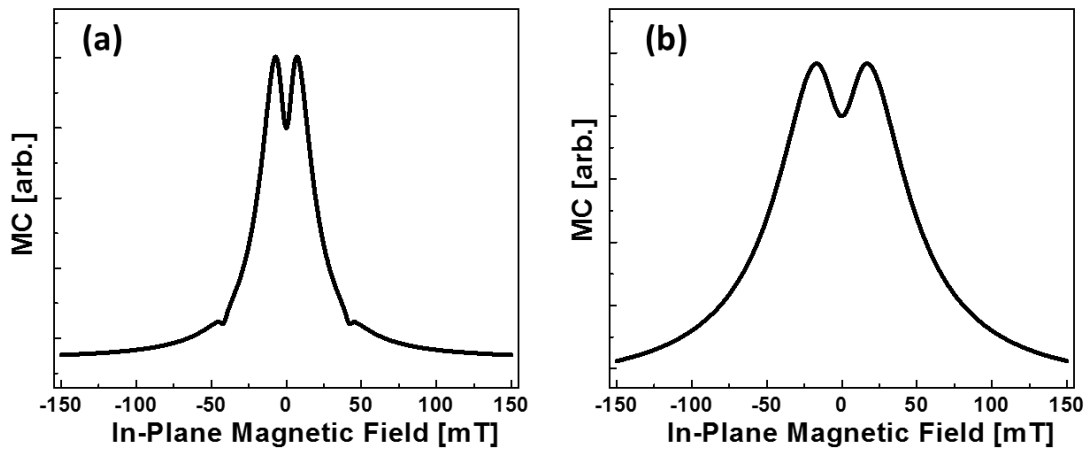


Figure 5

**Figure 5.** Angular dependence of magnetoconductance. Schematic illustration of the FET orientation to the applied magnetic field axis (top) and the measured MC response for different orientations of the FET ( $a$ - and  $b$ - axes plane of the tetracene crystal) to the magnetic field axis. Orientation angle is indicated as  $\theta$ . As indicated, the sample axis is defined as the axis vertically crossing two parallel electrodes. To set the field orientation, the sample axis was rotated. Angle between the crystal  $b$ -axis and the sample axis was around  $2^\circ$  and the crystal  $a$ -axis was perpendicular to the crystal  $b$ -axis (see Supporting Information).



**Figure 6**

**Figure 6.** Simulated magnetoconductance. MC response simulated for the singlet fission/triplet fusion processes in single crystal tetracene FETs with the magnetic field applied along (a)  $x$ -axis and (b)  $z$ -axis directions. Since  $x$ - and  $z$ -axes are closely aligned with the crystal  $a$ - and  $b$ -axes, respectively, the simulated MC curves plotted in (a) and (b) correspond to the measured MC curves of around  $\theta = 0^\circ$  and  $90^\circ$  of figure 5, respectively.

## ASSOCIATED CONTENT

**Supporting Information.** Figures S1 – S8 as described in the text, further analysis on electrical and magnetoconductance measurements of the devices, crystal axis measurement of tetracene, further details on mathematical calculation, and further discussion of proposed theoretical models. This material is available free of charge *via* the Internet at <http://pubs.acs.org>.

## AUTHOR INFORMATION

### **Corresponding Author**

\* [hjaejang@gmail.com](mailto:hjaejang@gmail.com)

## ACKNOWLEDGMENT

The authors would like to acknowledge Mr. O. A. Kirillov for assistance with the device fabrication, Dr. E. J. Heilweil and Dr. N. V. Nguyen for assistance and advice for the optical measurements, Dr. A. J. Barito and Dr. R. C. Bruce for technical advice, Dr. J. Campbell and Dr. S. Engmann for the critical reading and helpful discussion. Device fabrication was done in part at the NIST Center for Nanoscale Science and Technology. This work was performed in part under the financial assistance award 70NANB15H303 from the U.S. Department of Commerce, National Institute of Standards and Technology. Certain commercial equipment, instruments, or materials are identified in this paper in order to specify the experimental procedure adequately. Such identification is not intended to imply recommendation or endorsement by the National Institute

of Standards and Technology, nor is it intended to imply that the materials or equipment identified are necessarily the best available for the purpose.

## REFERENCES

1. Editorial, Why Going Organic is Good. *Nat. Mater.* **2009**, *8*, 691.
2. Jang, H.-J.; Richter, C. A. Organic Spin-Valves and Beyond: Spin Injection and Transport in Organic Semiconductors and the Effect of Interfacial Engineering. *Adv. Mater.* **2017**, *29*, 1602739-1602756.
3. Hu, B.; Yan, L.; Shao, M. Magnetic-Field Effects in Organic Semiconducting Materials and Devices. *Adv. Mater.* **2009**, *21*, 1500-1516.
4. Wagemans, W.; Janssen, P.; Schellekens, A. J.; Bloom, F. L.; Bobbert, P. A.; Koopmans, B. The Many Faces of Organic Magnetoresistance. *SPIN* **2011**, *01*, 93-108.
5. Zhang, Y.; Basel, T. P.; Gautam, B. R.; Yang, X.; Mascaro, D. J.; Liu, F.; Vardeny, Z. V. Spin-Enhanced Organic Bulk Heterojunction Photovoltaic Solar Cells. *Nat. Commun.* **2012**, *3*, 1043-1049.
6. Macià, F.; Wang, F.; Harmon, N. J.; Kent, A. D.; Wohlgenannt, M.; Flatté, M. E. Organic Magnetoelectroluminescence for Room Temperature Transduction between Magnetic and Optical Information. *Nat. Commun.* **2014**, *5*, 3609-3615.
7. Jang, H.-J.; Pookpanratana, S. J.; Brigeman, A. N.; Kline, R. J.; Basham, J. I.; Gundlach, D. J.; Hacker, C. A.; Kirillov, O. A.; Jurchescu, O. D.; Richter, C. A. Interface Engineering to

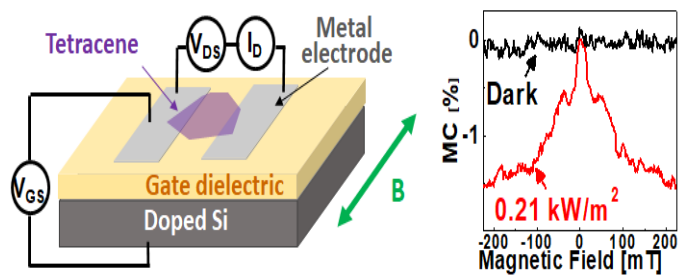
- Control Magnetic Field Effects of Organic-Based Devices by Using a Molecular Self-Assembled Monolayer. *ACS Nano* **2014**, *8*, 7192-7201.
8. Kalinowski, J.; Godlewski, J. Magnetic Field Effects on Recombination Radiation in Tetracene Crystal. *Chem. Phys. Lett.* **1975**, *36*, 345-348.
  9. Geacintov, N.; Pope, M.; Vogel, F. Effect of Magnetic Field on the Fluorescence of Tetracene Crystals: Exciton Fission. *Phys. Rev. Lett.* **1969**, *22*, 593-596.
  10. Burdett, J. J.; Piland, G. B.; Bardeen, C. J. Magnetic Field Effects and the Role of Spin States in Singlet Fission. *Chem. Phys. Lett.* **2013**, *585*, 1-10.
  11. Wakasa, M.; Kaise, M.; Yago, T.; Katoh, R.; Wakikawa, Y.; Ikoma, T. What Can Be Learned from Magnetic Field Effects on Singlet Fission: Role of Exchange Interaction in Excited Triplet Pairs. *J. Phys. Chem. C* **2015**, *119*, 25840-25844.
  12. Rybicki, J.; Lin, R.; Wang, F.; Wohlgenannt, M.; He, C.; Sanders, T.; Suzuki, Y. Tuning the Performance of Organic Spintronic Devices Using X-Ray Generated Traps. *Phys. Rev. Lett.* **2012**, *109*, 076603-076607.
  13. Singh, S.; Jones, W. J.; Siebrand, W.; Stoicheff, B. P.; Schneider, W. G. Laser Generation of Excitons and Fluorescence in Anthracene Crystals. *J. Chem. Phys.* **1965**, *42*, 330-342.
  14. Swenberg, C. E.; Stacy, W. T. Bimolecular Radiationless Transitions in Crystalline Tetracene. *Chem. Phys. Lett.* **1968**, *2*, 327-328.
  15. Merrifield, R. E.; Avakian, P.; Groff, R. P. Fission of Singlet Excitons into Pairs of Triplet Excitons in Tetracene Crystals. *Chem. Phys. Lett.* **1969**, *3*, 386-388.

16. Chan, W.-L.; Berkelbach, T. C.; Provorse, M. R.; Monahan, N. R.; Tritsch, J. R.; Hybertsen, M. S.; Reichman, D. R.; Gao, J.; Zhu, X. Y. The Quantum Coherent Mechanism for Singlet Fission: Experiment and Theory. *Acc. Chem. Res.* **2013**, *46*, 1321-1329.
17. Wilson, M. W. B.; Rao, A.; Ehrler, B.; Friend, R. H. Singlet Exciton Fission in Polycrystalline Pentacene: from Photophysics toward Devices. *Acc. Chem. Res.* **2013**, *46*, 1330-1338.
18. Zhang, B.; Zhang, C.; Wang, R.; Tan, Z.; Liu, Y.; Guo, W.; Zhai, X.; Cao, Y.; Wang, X.; Xiao, M. Nonlinear Density Dependence of Singlet Fission Rate in Tetracene Films. *J. Phys. Chem. Lett.* **2014**, *5*, 3462-3467.
19. Smith, M. B.; Michl, J. Recent Advances in Singlet Fission. *Annu. Rev. Phys. Chem.* **2013**, *64*, 361-386.
20. Piland, G. B.; Burdett, J. J.; Dillon, R. J.; Bardeen, C. J. Singlet Fission: from Coherences to Kinetics. *J. Phys. Chem. Lett.* **2014**, *5*, 2312-2319.
21. Burdett, J. J.; Bardeen, C. J. The Dynamics of Singlet Fission in Crystalline Tetracene and Covalent Analogs. *Acc. Chem. Res.* **2013**, *46*, 1312-1320.
22. Congreve, D.N.; Lee, J.; Thompson, N.J.; Hontz, E.; Yost, S.R.; Reuswig, P.D.; Bahlke, M.E.; Reineke, S.; Voorhis, T.V.; Baldo, M.A. External Quantum Efficiency Above 100% in a Singlet-Exciton-Fission-Based Organic Photovoltaic Cell. *Science* **2013**, *340*, 334-337.
23. Tatarov, E.; Reichert, T.; Saragi, T. P. I.; Scheffler, A.; Ueberschaer, R.; Bruhn, C.; Fuhrmann-Lieker, T.; Salbeck, J. Photoinduced Sign Change of the Magnetoresistance in

- Field-Effect Transistors Based on a Bipolar Molecular Glass. *Chem. Commun.* **2013**, *49*, 4564-4566.
24. Yutaka, W.; Ryoma, H.; Hoon-Seok, S. Recent Progress in Photoactive Organic Field-Effect Transistors. *Sci. Technol. Adv. Mater.* **2014**, *15*, 024202-024220.
25. Geacintov, N.; Pope, M.; Kallmann, H. Photogeneration of Charge Carriers in Tetracene. *J. Chem. Phys.* **1966**, *45*, 2639-2649.
26. Geacintov, N. E.; Pope, M.; Fox, S. Magnetic Field Effects on Photo-Enhanced Currents in Organic Crystals. *J. Phys. Chem. Solids* **1970**, *31*, 1375-1379.
27. Saragi, T. P. I.; Reichert, T. Magnetic-Field Effects in Illuminated Tetracene Field-Effect Transistors. *Appl. Phys. Lett.* **2012**, *100*, 073304-073307.
28. Geacintov, N. E.; Binder, M.; Swenberg, C. E.; Pope, M. Exciton Dynamics in  $\alpha$ -Particle Tracks in Organic Crystals: Magnetic Field Study of the Scintillation in Tetracene Crystals. *Phys. Rev. B* **1975**, *12*, 4113-4134.
29. Yakovlev, B. S.; Novikova, L. I.; Frankevich, E. L. Photogeneration of Current Carriers in Crystalline Tetracene in a Magnetic Field. *J. Exp. Theor. Phys.* **1970**, *31*, 4-7.
30. Bree, A.; Lyons, L. E. 1002. The Intensity of Ultraviolet-Light Absorption by Monocrystals. Part IV. Absorption by Naphthacene of Plane-Polarized Light. *J. Chem. Soc. (Resumed)* **1960**, 5206-5212.
31. Wilson, M. W. B.; Rao, A.; Johnson, K.; Gélinas, S.; di Pietro, R.; Clark, J.; Friend, R. H. Temperature-Independent Singlet Exciton Fission in Tetracene. *J. Am. Chem. Soc.* **2013**, *135*, 16680-16688.

32. Sternlicht, H.; McConnell, H. M. Paramagnetic Excitons in Molecular Crystals. *J. Chem. Phys.* **1961**, *35*, 1793-1800.
33. Yarmus, L.; Rosenthal, J.; Chopp, M. EPR of Triplet Excitations in Tetracene Crystals: Spin Polarization and the Role of Singlet Exciton Fission. *Chem. Phys. Lett.* **1972**, *16*, 477-481.
34. Wang, R.; Zhang, C.; Zhang, B.; Liu, Y.; Wang, X.; Xiao, M. Magnetic Dipolar Interaction between Correlated Triplets Created by Singlet Fission in Tetracene Crystals. *Nat. Commun.* **2015**, *6*, 8602-8607.
35. Podzorov, V. Charge Carrier Transport in Single-Crystal Organic Field-Effect Transistors. In *Organic Field-Effect Transistors*, CRC Press: **2007**; pp 27-72.
36. Timmel, C. R.; Till, U.; Brocklehurst, B.; McLauchlan, K. A.; Hore, P. J. Effects of Weak Magnetic Fields on Free Radical Recombination Reactions. *Mol. Phys.* **1998**, *95*, 71-89.
37. Nguyen, T. D.; Gautam, B. R.; Ehrenfreund, E.; Vardeny, Z. V. Magnetoconductance Response in Unipolar and Bipolar Organic Diodes at Ultrasmall Fields. *Phys. Rev. Lett.* **2010**, *105*, 166804-166807.
38. Pernstich, K. P.; Haas, S.; Oberhoff, D.; Goldmann, C.; Gundlach, D. J.; Batlogg, B. Threshold Voltage Shift in Organic Field Effect Transistors by Dipole Monolayers on the Gate Insulator. *J. Appl. Phys.* **2004**, *96*, 6431-6438.
39. Goldmann, C.; Krellner, C.; Pernstich, K. P.; Haas, S.; Gundlach, D. J.; Batlogg, B. Determination of the Interface Trap Density of Rubrene Single-Crystal Field-Effect Transistors and Comparison to the Bulk Trap Density. *J. Appl. Phys.* **2006**, *99*, 034507-034514.

## Graphical Table of Contents



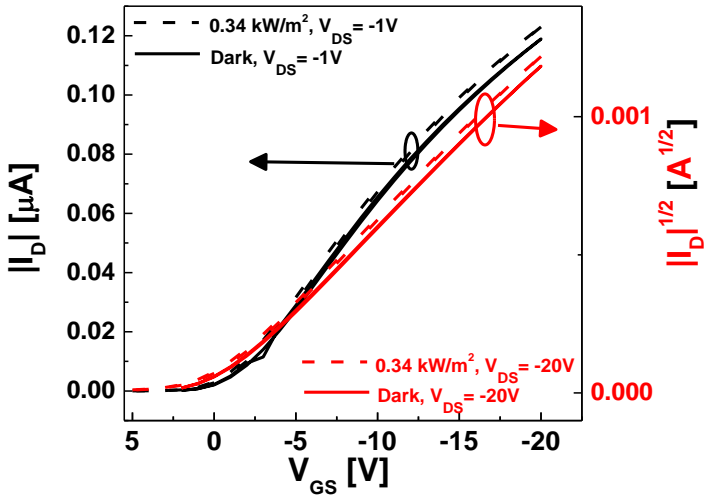
# Supporting Information

## Electrical Detection of Singlet Fission in Single Crystal Tetracene Transistors

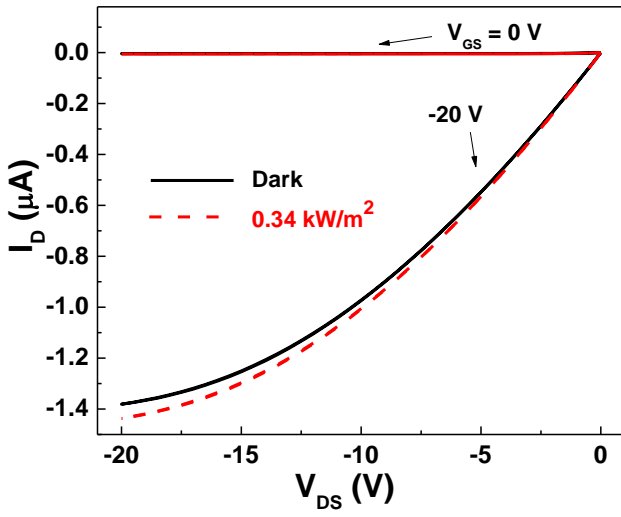
*Hyuk-Jae Jang,<sup>†,‡,§,\*</sup> Emily G. Bittle,<sup>‡</sup> Qin Zhang,<sup>†,‡</sup> Adam J. Biacchi,<sup>‡</sup> Curt A. Richter,<sup>‡</sup> and  
David J. Gundlach<sup>‡</sup>*

<sup>†</sup>Theiss Research, La Jolla, CA 92037, USA. <sup>‡</sup>Nanoscale Device Characterization Division,  
National Institute of Standards and Technology, 100 Bureau Drive, Gaithersburg, MD 20899,  
USA. <sup>§</sup>Western Digital Corporation, 5601 Great Oaks Parkway, San Jose, CA 95119, USA.

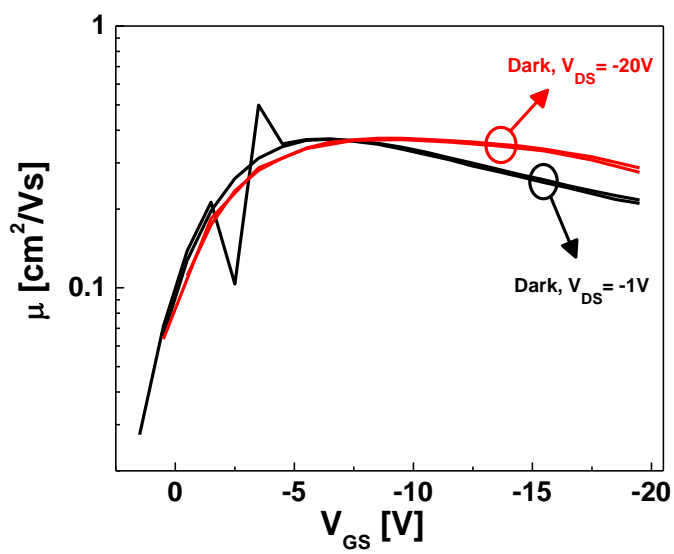
**a**



b



c



d

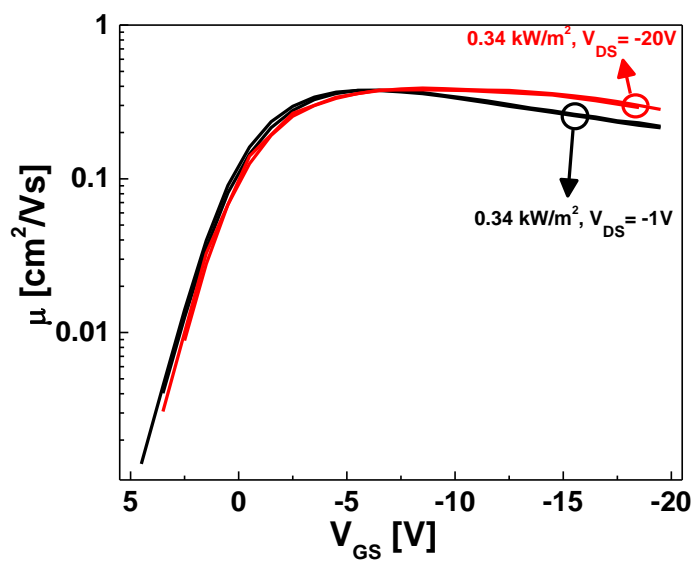
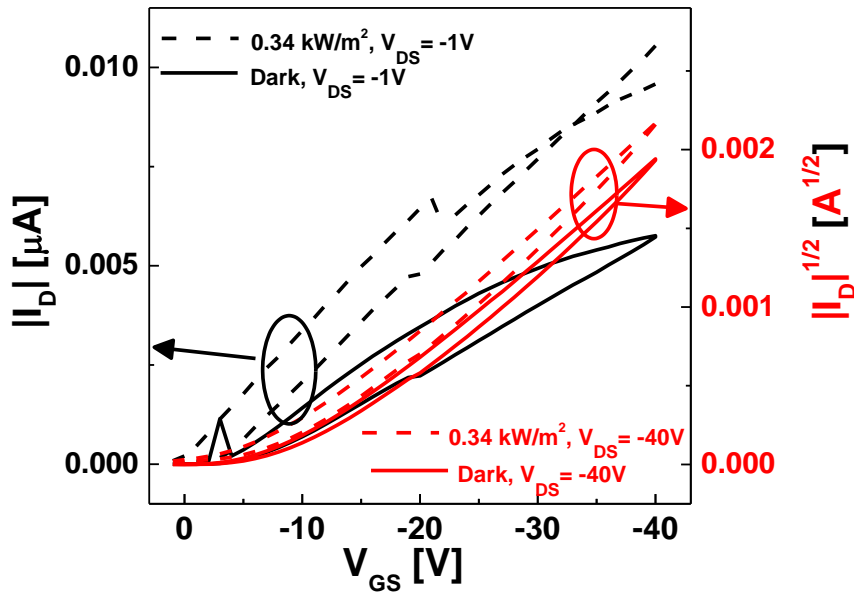


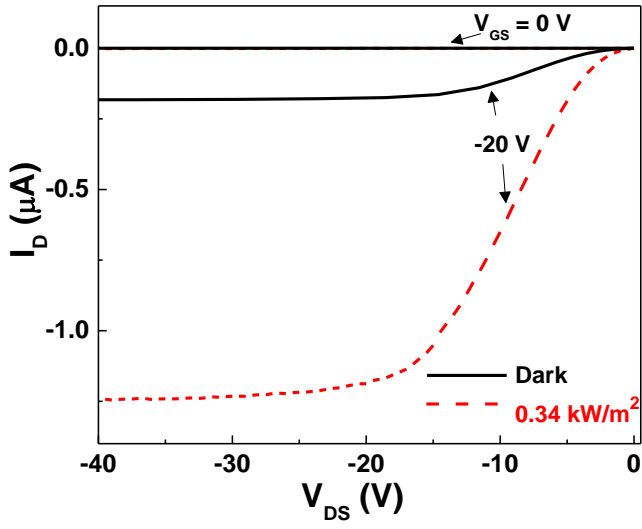
**Figure S1.** Electrical characteristics of single crystalline tetracene field effect transistor (FET) made on Cytop gate dielectric: (a) Drain current ( $I_D$ ) *versus* gate bias ( $V_{GS}$ ) at  $V_{DS}$  (drain-source voltage) = -1 V (linear regime) (black lines) and square root of  $I_D$  *versus*  $V_{GS}$  at  $V_{DS}$  = -20 V

(saturation regime) (red lines). (b) Drain current,  $I_D$  versus drain-source voltage,  $V_{DS}$  of a single crystalline tetracene FET measured at 0 V and -20 V of gate bias,  $V_{GS}$  in darkness (solid black lines) and under illumination intensity of  $0.34 \text{ kW/m}^2$  (dotted red lines). The channel distance between drain and source was  $50 \text{ }\mu\text{m}$ . (c) Differential mobility of a single crystalline tetracene field effect transistor (FET) in darkness with drain-source voltage ( $V_{DS}$ ) of -1 V (linear regime, black line) and -20 V (saturation regime, red line). (d) Differential mobility of a single crystalline tetracene field effect transistor (FET) under illumination intensity of  $0.34 \text{ kW/m}^2$  with drain-source voltage ( $V_{DS}$ ) of -1 V (linear regime, black line) and -20 V (saturation regime, red line).

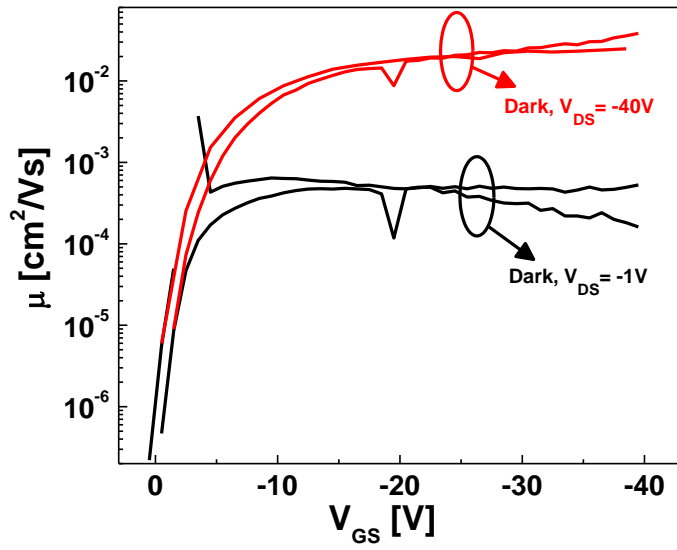
a



b



c



d

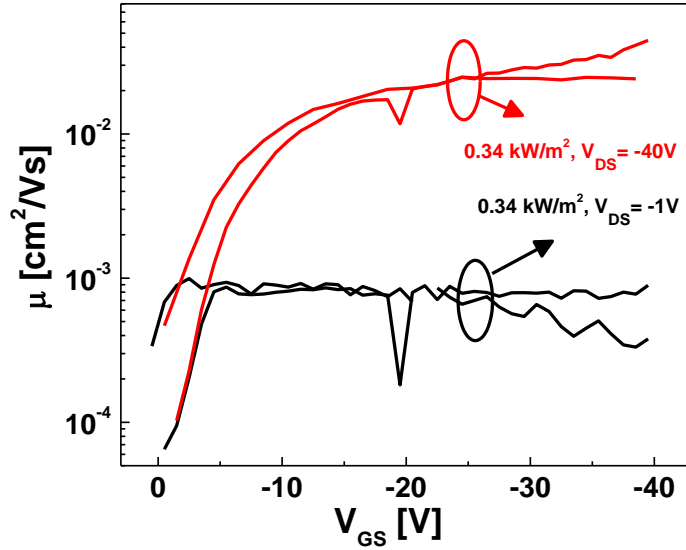
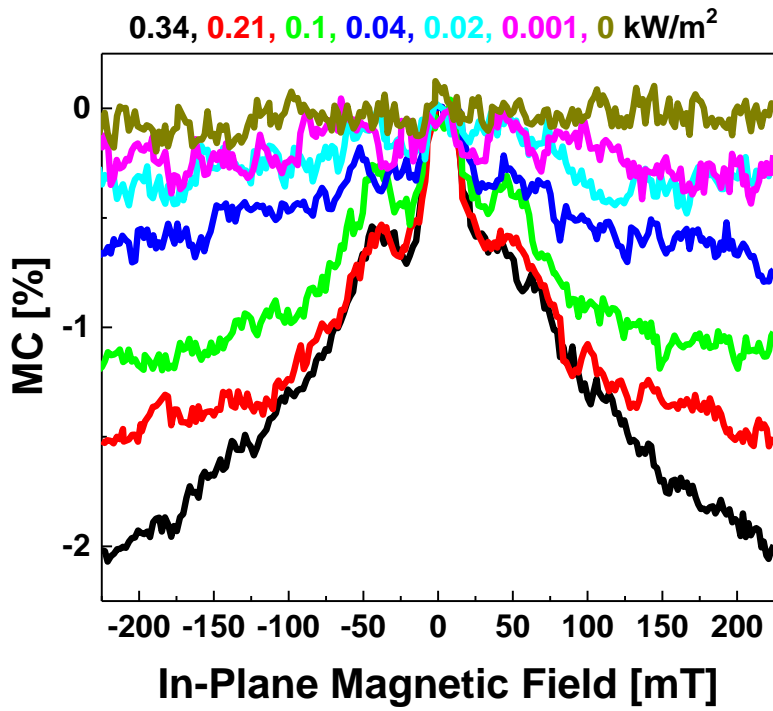


**Figure S2.** Electrical characteristics of single crystalline tetracene FET made on  $\text{SiO}_2$  gate dielectric: (a) Drain current ( $I_D$ ) versus gate bias ( $V_{GS}$ ) at  $V_{DS}$  (drain-source voltage) = -1 V (linear regime) (black lines) and square root of  $I_D$  versus  $V_{GS}$  at  $V_{DS} = -40\text{ V}$  (saturation regime) (red lines). (b) Drain current,  $I_D$  versus drain-source voltage,  $V_{DS}$  of a single crystalline tetracene FET measured at 0 V and -20 V of gate bias,  $V_{GS}$  in darkness (solid black lines) and under illumination intensity of  $0.34\text{ kW/m}^2$  (dotted red lines). The channel distance between drain and source was  $10\text{ }\mu\text{m}$ . Data under illumination and in darkness obtained in different dates, respectively, and thus they cannot be directly compared for illumination effect. (c) Differential mobility of a single crystalline tetracene field effect transistor (FET) in darkness with drain-source voltage ( $V_{DS}$ ) of -1 V (linear regime, black line) and -40 V (saturation regime, red line). (d) Differential mobility of a single crystalline tetracene field effect transistor (FET) under illumination intensity of  $0.34\text{ kW/m}^2$  with drain-source voltage ( $V_{DS}$ ) of -1 V (linear regime, black line) and -40 V (saturation regime, red line).

As shown in Figure S1c and S1d, our single crystalline tetracene field effect transistor (FET) prepared on Cytop gate dielectric had much higher mobility than previously reported thin film tetracene FETs.<sup>1</sup> The mobility of our tetracene FETs decreased when they were prepared on SiO<sub>2</sub> gate dielectric as displayed in Figure S2c and S2d, but it was still higher than that of previously reported thin film tetracene FETs. The transistor made on SiO<sub>2</sub> gate dielectric, shows  $\mu \sim V_{GS}^N$  dependence, which is commonly associated with a broad distribution of available electronic states near the HOMO level of amorphous p-type polymer semiconductors.<sup>2,3</sup> This type of behavior can be induced in single crystals when there are a large number of trapping sites, indicated by the very low mobility in the linear regime. While the transistors made on SiO<sub>2</sub> gate dielectric in our study show this behavior, when made on Cytop (a fluoropolymer dielectric material) gate dielectric that shows low interface trapping,<sup>4</sup> we did not observe this behavior and ideal transistor behavior was obtained. Therefore, we believe that the additional trapping states in these transistors is due to states induced by either water trapping or dangling H<sub>2</sub> bonds at the SiO<sub>2</sub>/tetracene interface.

**a.**



b.

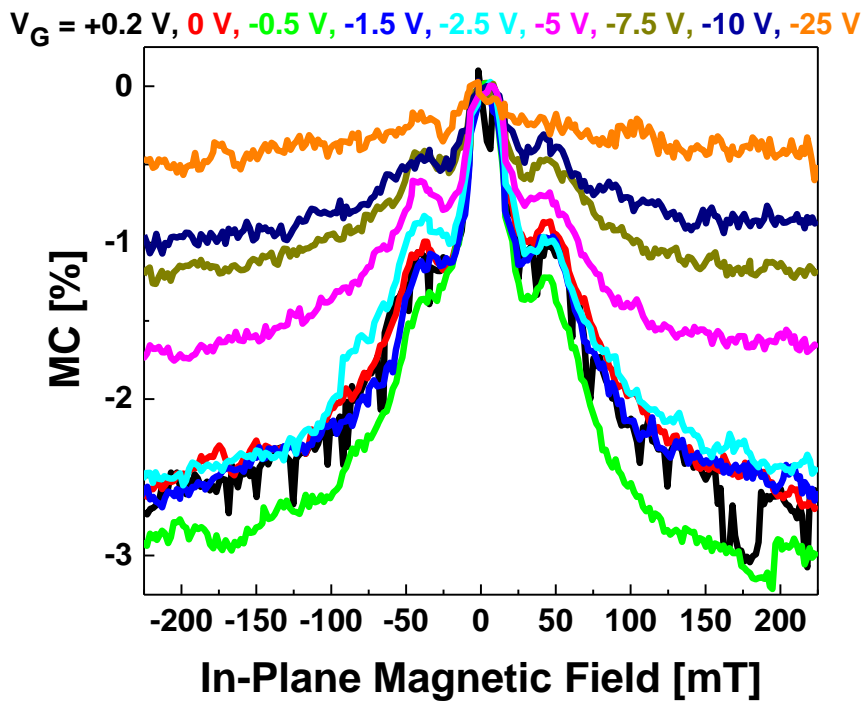


**Figure S3.** Magnetoconductance of a single crystal tetracene FET fabricated with SiO<sub>2</sub> gate dielectric: (a) under illumination with different intensities and with  $V_{DS} = -20$  V and  $V_{GS} = -2.5$  V. (b) with different  $V_{GS}$  under the illumination intensity of 0.34 kW/m<sup>2</sup> with  $V_{DS} = -20$  V. The device channel length was 10  $\mu$ m. The MC was defined as  $[I_{DS}(B) - I_{DS}(B = 0)] / I_{DS}(B = 0)$ , where B is the magnetic field strength.

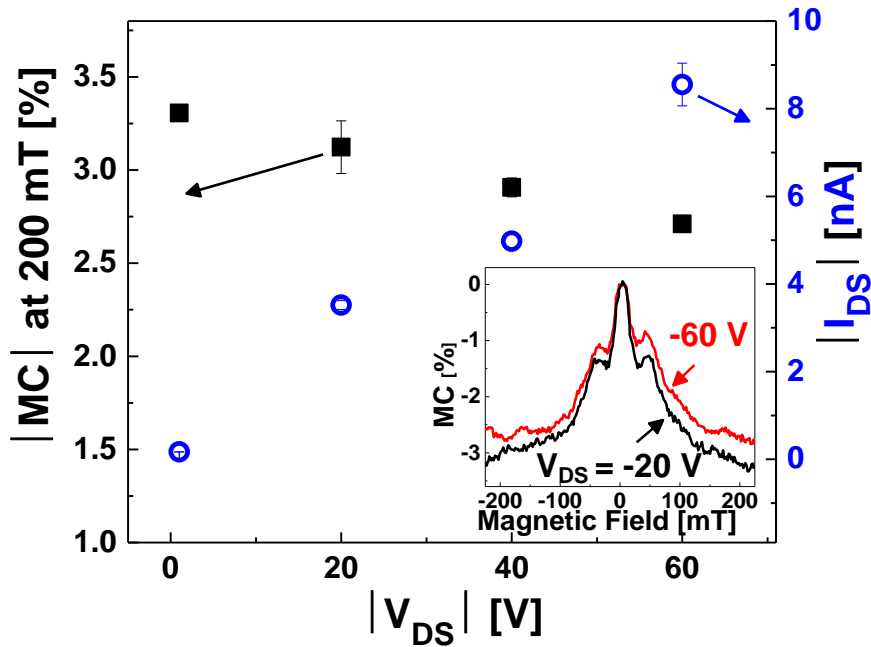


**Figure S4.** Magnitude of magnetoconductance (MC),  $|MC|$  at the magnetic field of 200 mT (black filled squares) and the magnitude of  $I_{DS}$ ,  $|I_{DS}|$  (blue open circles) *versus* the magnitude of  $V_{DS}$ ,  $|V_{DS}|$  measured in the FET prepared on SiO<sub>2</sub> gate dielectric with a channel length of 10  $\mu$ m. The MC was defined as  $[I_{DS}(B) - I_{DS}(B = 0)] / I_{DS}(B = 0)$ , where B is the magnetic field

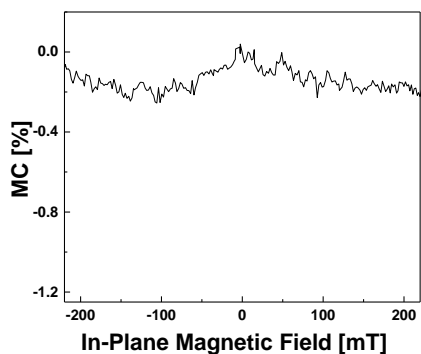
strength. Inset: MC measured with  $V_{DS} = -20$  V (black line) and  $-60$  V (red line) under the illumination intensity of  $0.34$  kW/m<sup>2</sup> with  $V_G = -2.5$  V.

Figure S4 displays the changes in the  $|MC|$  and the  $|I_{DS}|$  by varying the  $V_{DS}$ . We found that the  $|MC|$  became slightly smaller when the magnitude of  $V_{DS}$  ( $|V_{DS}|$ ) increased even though there was a significant increment in the  $|I_{DS}|$  (in the linear regime prior to the saturation regime). A small decrease in the  $|MC|$  at higher  $|V_{DS}|$  may have resulted from the reduction in the rate of interaction between free charge carriers and triplet excitons due to the charge carriers' shorter transit time. A decrement in the interaction between free charge carriers and triplet excitons reduces the contribution of triplet dissociation into secondary charge carriers to photo-generated current, and thus the  $|MC|$  decreases since the formation of triplet excitons in tetracene is magnetic field dependent. A small reduction in the  $|MC|$  despite a large increase  $|I_{DS}|$  at high  $|V_{DS}|$  suggests that the contribution of triplet dissociation into secondary charge carriers by the interaction with free charge carriers to magnetic field dependent photo-induced current is quite small in the tetracene FETs.

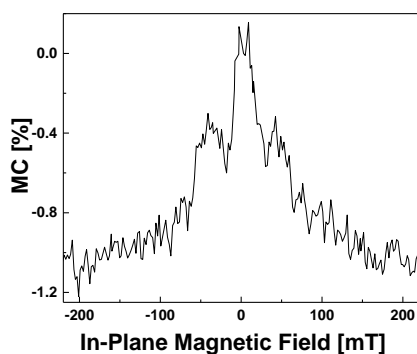
Contact resistance typically decreases as  $|V_{DS}|$  becomes larger and contact resistance becomes very small in a regime at large  $|V_{DS}|$  with  $V_{GS} < 0$ . Our data show that there is only slight decrease in magnetoconductance even at high  $|V_{DS}|$  indicating that contact resistance may not be an important factor for the magnetoconductance measurement.<sup>5</sup>

**a**

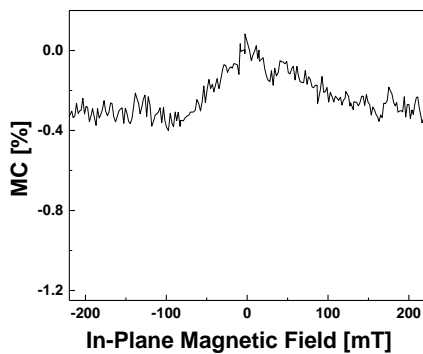
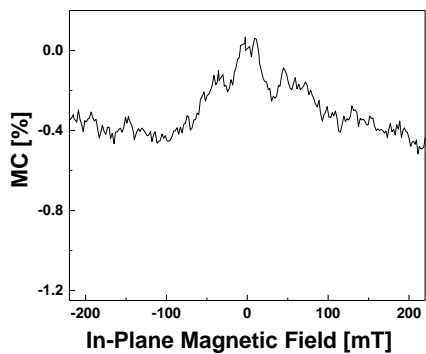
**b**



c



d



e

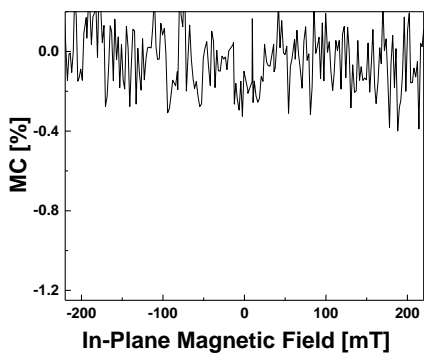


**Figure S5.** Magnetoconductance (MC) of a single crystalline tetracene field effect transistor (FET) under the light illumination optically filtered with different wavelengths. Broadband light was transmitted through (a) 400 nm short pass filter, (b) 385 nm long pass filter, (c) 495 nm long

pass filter, (d) 570 nm long pass filter, and (e) 615 nm long pass filter. The channel distance between drain and source of the FET was 10  $\mu\text{m}$ .

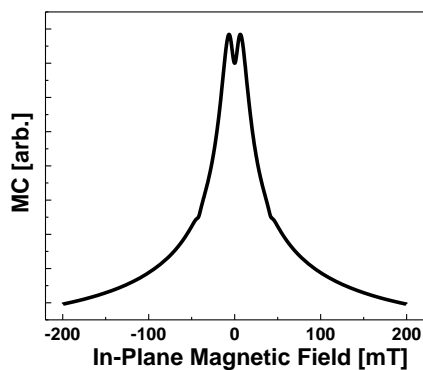
	400 nm short pass	385 nm long pass	495 nm long pass	570 nm long pass	615 nm long pass
$(I_D)_{\text{filtered}} /$ $(I_D)_{\text{unfiltered}}$	$0.408 \pm$	$0.868 \pm$	$0.664 \pm$	$0.389 \pm$	$0.360 \pm$
$(I_D)_{\text{filtered}} /$ $(I_D)_{\text{darkness}}$	$1.24 \pm 0.03$	$2.63 \pm 0.02$	$2.01 \pm 0.02$	$1.18 \pm 0.04$	$1.09 \pm 0.04$

**Table S1.** Ratio between drain current ( $I_D$ ) under the optically filtered illumination with different wavelengths and  $I_D$  under the unfiltered light of  $0.34 \text{ kW/m}^2$  (second row) and in darkness (third row). Gate bias ( $V_{GS}$ ) of  $-1.5 \text{ V}$  and drain-source voltage ( $V_{DS}$ ) of  $-0.4 \text{ V}$  were applied for the measurements.

Figure S5 illustrates the measured magnetoconductance (MC) of a single crystalline tetracene field effect transistor (FET) under the optically filtered light illumination with various wavelengths at room temperature. Due to aging and degradation of the device, the magnitude of MC was smaller and its signal was noisier during the wavelength dependence measurements than during all the previously carried out measurements described in the main manuscript, but MC of larger than 1.5% was still probed under the unfiltered illumination of  $0.34 \text{ kW/m}^2$ . MC was clearly seen under the filtered illumination with 385 nm, 495 nm, and 570 nm long pass filters

and also, with a 400 nm short pass filter, but no sign of MC was detected with a 615 nm long pass filter. Since our unfiltered optic illuminator has a spectrum of wavelengths that range from  $\approx 350$  nm to  $\approx 1400$  nm, we reached the conclusion that the light with wavelengths between  $\approx 350$  nm and  $\approx 615$  nm are responsible for the observed photo-induced MC in our tetracene FETs. Our conclusion agrees with a previous result, which reported that the relative change between photocurrent in a tetracene with a magnetic field of 200 mT and that without a magnetic field was observed only with the wavelength of the light between 350 nm and 615 nm.<sup>6</sup> Table S1 displays the relative change of drain-source current ( $I_D$ ) under the filtered illumination with respect to the unfiltered light and darkness. We observed that the magnitude of photocurrent,  $I_D$  drastically decreased above 570 nm. Previous reports on absorption spectrum of tetracene support our experimental data showing that light absorption was greatly reduced with the wavelength above  $\approx 560$  nm and below  $\approx 400$  nm.<sup>7, 8</sup>

**a**



**b**

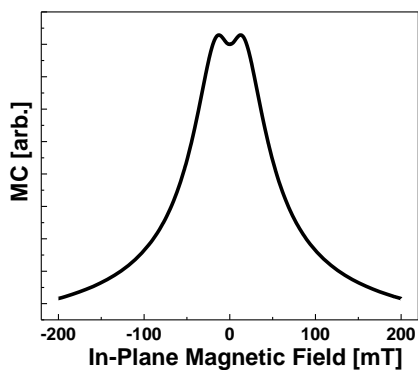


**Figure S6.** Calculated MC curves of single crystalline tetracene FETs taking both singlet fission process and the intersystem crossing by random hyperfine fields into account when the magnetic field is applied along (a)  $x$ -axis and (b)  $z$ -axis.

As briefly discussed in the main manuscript, it was previously reported that the intersystem crossing caused by random hyperfine fields in organic semiconductor based systems can also generate magnetoconductance (MC) and the MC can be well fit with either Lorentzian ( $B^2/(B_0^2+B^2)$ ) or non-Lorentzian ( $B^2/(B_0+|B|)^2$ ) equations.<sup>9, 10</sup> In these equations,  $B_0$  is known to be related to the strength of hyperfine interaction.<sup>9, 10</sup> If the intersystem crossing induced by random hyperfine fields occurs in addition to singlet fission, one may add a Lorentzian or non-Lorentzian model to the singlet fission model which was discussed in the main manuscript. Figure S6 illustrates the results (simulated MC curves obtained by combining two models). In this simulation, we found that an addition of an empirical non-Lorentzian ( $B^2/(B_0+|B|)^2$ ) model with  $B_0 = 30$  mT helped the general shape of simulated MC curves become more similar to experimentally obtained MC curves along both  $x$ -axis and  $z$ -axis. (However, the size of humps around the magnetic field of 42 mT in MC curves became much smaller by introducing a non-Lorentzian model because the MC signal induced by the singlet fission is diluted.) The relative strength of MC between the non-Lorentzian model and the singlet fission model used in the calculation was 1:2. Our results imply that in order to construct the simulated MC fully replicating the experimentally observed MC, one may need more sophisticated model involving other magnetic field dependent mechanisms or processes.<sup>6</sup>

**a**

**b**

**c**

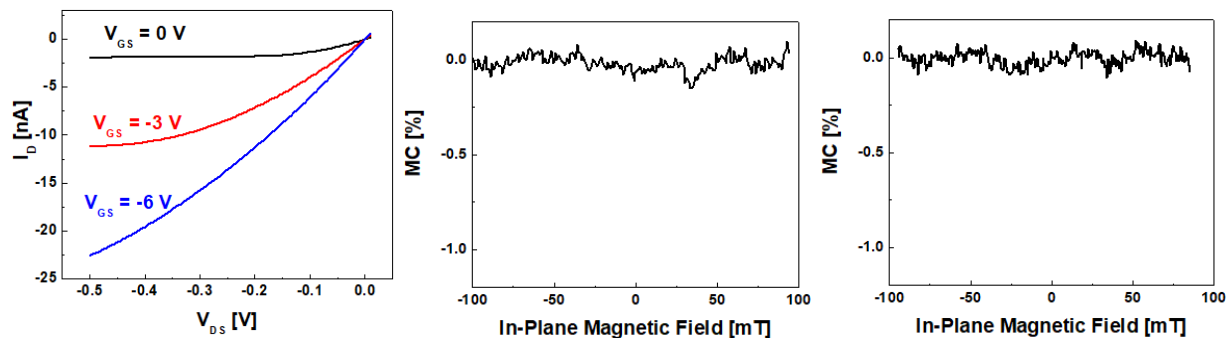


**Figure S7.** (a) Drain current,  $I_D$  versus drain-source voltage,  $V_{DS}$  of a P3HT thin film FET measured at 0 V (black), -3 V (red), and -6 V (blue) of gate bias,  $V_{GS}$  in darkness.

Magnetoconductance (MC) of a P3HT thin film FET (b) in darkness and (c) under illumination with intensity of 0.34 kW/m<sup>2</sup>. Both MC measurements were carried out with  $V_{DS} = -0.1$  V and  $V_{GS} = -0.1$  V. The MC was defined as  $[I_{DS}(B) - I_{DS}(B = 0)] / I_{DS}(B = 0)$ , where B is the magnetic field strength. The channel distance between drain and source was 5  $\mu\text{m}$ .

We also investigated the magnetoconductance (MC) of FETs made of organic semiconducting systems such as P3HT and PCBM where singlet fission process does not exist. However, we were not able to observe any MC effect either under illumination or in darkness as illustrated in Figure S7.

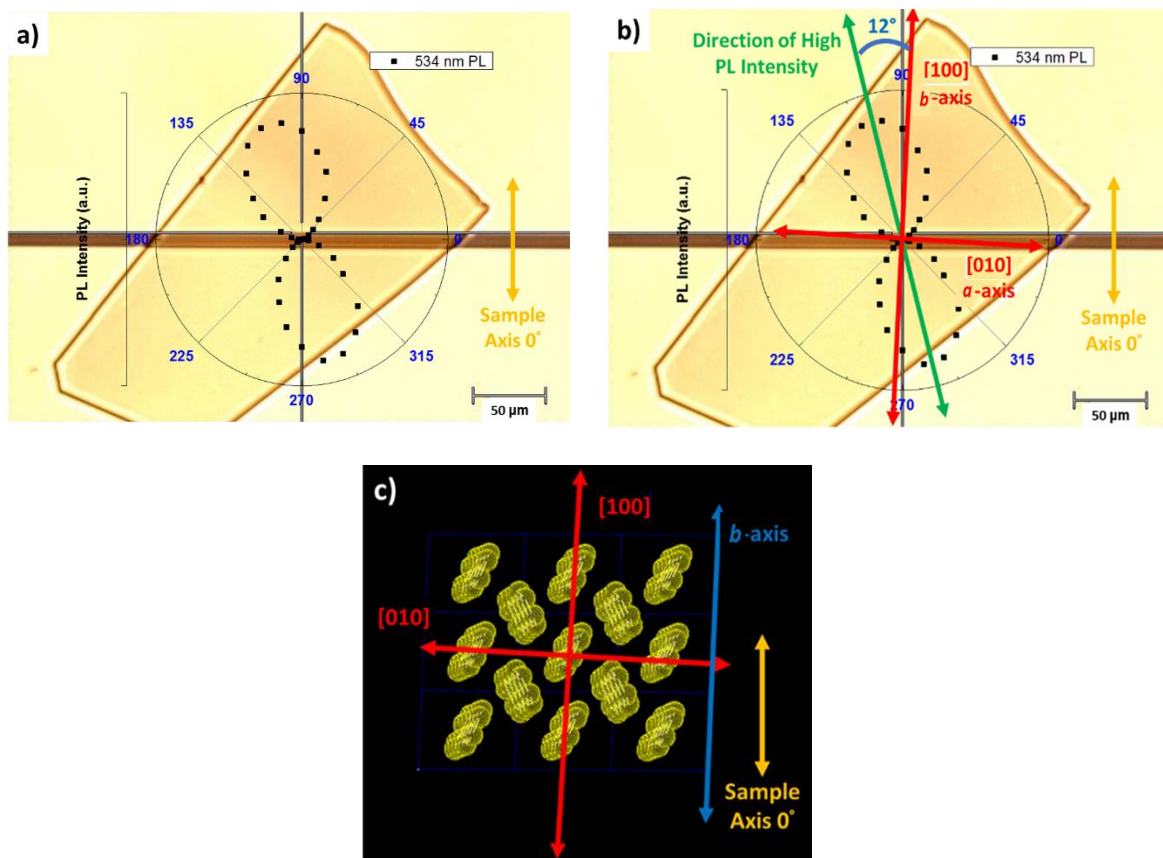


**Figure S8.** a) Angle-resolved photoluminescence measurement of the tetracene field-effect transistor device collected in the parallel polarization configuration. b) Results indicate that the sample axis of 0 degrees corresponds closely to the *b*-axis of single-crystalline tetracene. c) Crystal structure of single-crystalline tetracene oriented in the same direction as the field-effect transistor device.

We carried out photoluminescence (PL) spectroscopy to determine the orientation of the tetracene crystal used in our experiment as illustrated in Figure S8. Parallel-polarized, angle-dependent PL spectra were collected at room temperature in the 180° backscattering configuration through a confocal microscope (50x objective) coupled to a Renishaw inVia

spectrometer (1200 lines / mm). The excitation source was a linearly polarized 514 nm Ar+ laser (100  $\mu$ W). Backscattered PL was collected through a polarizer set parallel to the incident polarization at a collection time of 1 s. The sample was rotated in increments of 10° and the PL intensity at 534 nm was monitored. As determined previously by our group<sup>11</sup> and others,<sup>12</sup> the [100] crystallographic direction, corresponding to the is the single-crystalline *b*-axis, is approximately 12 ° off angle of the highest PL intensity in our tetracene FET. Our results indicate the *b*-axis lies close to the zero-degree sample axis.

### Mathematical details of theoretical model calculation

Given spin matrices  $S_x$ ,  $S_y$ , and  $S_z$ , where

$$S_x = \frac{\hbar}{\sqrt{2}} \begin{pmatrix} 0 & 1 & 0 \\ 1 & 0 & 1 \\ 0 & 1 & 0 \end{pmatrix}, S_y = \frac{\hbar}{\sqrt{2}} \begin{pmatrix} 0 & -i & 0 \\ i & 0 & -i \\ 0 & i & 0 \end{pmatrix}, S_z = \hbar \begin{pmatrix} 1 & 0 & 0 \\ 0 & 0 & 0 \\ 0 & 0 & -1 \end{pmatrix},$$

one can evaluate the spin Hamiltonian  $H$  described in equation (1) of the main manuscript as follows:

$$H = \begin{pmatrix} \frac{1}{3}\hbar^2 D^* + g\mu_B \hbar B_z & g\mu_B \hbar \frac{(B_x - iB_y)}{\sqrt{2}} & \hbar E^* \\ g\mu_B \hbar \frac{(B_x + iB_y)}{\sqrt{2}} & -\frac{2}{3}\hbar^2 D^* & g\mu_B \hbar \frac{(B_x - iB_y)}{\sqrt{2}} \\ \hbar E^* & g\mu_B \hbar \frac{(B_x + iB_y)}{\sqrt{2}} & \frac{1}{3}\hbar^2 D^* - g\mu_B \hbar B_z \end{pmatrix}$$

When the external magnetic field is applied along *x*-axis,  $\mathbf{B} = B \mathbf{x}$  and the diagonalization of the Hamiltonian  $H$  produces the three eigenvalues,

$$\frac{1}{3}(\hbar^2 D^* - 3\hbar E^*), \frac{1}{6}(-\hbar^2 D^* + 3\hbar E^* - 3\sqrt{4(g\mu_B \hbar B)^2 + (\hbar^2 D^*)^2 + 2(\hbar^3 D^* E) + (\hbar E^*)^2}), \text{ and}$$

$$\frac{1}{6}(-\hbar^2 D^* + 3\hbar E^* + 3\sqrt{4(g\mu_B \hbar B)^2 + (\hbar^2 D^*)^2 + 2(\hbar^3 D^* E) + (\hbar E^*)^2}).$$

When the external magnetic field is applied along *z*-axis,  $\mathbf{B} = B \mathbf{z}$  and the diagonalization of the Hamiltonian  $H$  produces the three eigenvalues,

$$\frac{-2}{3}\hbar^2 D^*, \frac{1}{3}(\hbar^2 D^* - 3\sqrt{(g\mu_B \hbar B)^2 + (\hbar E^*)^2}), \text{ and } \frac{1}{3}(\hbar^2 D^* + 3\sqrt{(g\mu_B \hbar B)^2 + (\hbar E^*)^2}).$$

The eigenstates of the Hamiltonian described in equation (1) of the main manuscript when  $\mathbf{B} = 0$ ,  $|x_0\rangle$ ,  $|y_0\rangle$ , and  $|z_0\rangle$  can be obtained as  $(1/\sqrt{2})\{-1, 0, 1\}$ ,  $(1/\sqrt{2})\{i, 0, i\}$ , and  $\{0, 1, 0\}$ , respectively, which will produce  $|S^1\rangle = (1/\sqrt{3})(|x_0\rangle|x_0\rangle + |y_0\rangle|y_0\rangle + |z_0\rangle|z_0\rangle)$  for the evaluation of the equations (3) and (4) in the main text.

## References

1. Saragi, T.P.I.; Reichert, T. Magnetic-Field Effects in Illuminated Tetracene Field-Effect Transistors. *Appl. Phys. Lett.* **2012**, *100*, 073304-073307.
2. Vissenberg, M.C.J.M.; Matters, M. Theory of the Field-Effect Mobility in Amorphous Organic Transistors. *Phys. Rev. B* **1998**, *57*, 12964-12967.
3. Bittle, E.G.; Ro, H.W.; Snyder, C.R.; Engmann, S.; Kline, R.J.; Zhang, X.; Jurchescu, O.D.; DeLongchamp, D.M.; Gundlach, D.J. Dependence of Electrical Performance on Structural Organization in Polymer Field Effect Transistors. *J. Polym. Sci. B: Polym. Phys.*, **2017**, *55*, 1063-1074.
4. Blülle, B.; Häusermann, R.; Batlogg, B. Approaching the Trap-Free Limit in Organic Single-Crystal Field-Effect Transistors. *Phys. Rev. Appl.* **2014**, *1*, 034006-034013.
5. Podzorov, V. Charge Carrier Transport in Single-Crystal Organic Field-Effect Transistors. In *Organic Field-Effect Transistors*, CRC Press: **2007**; pp 27-72.
6. Yakovlev, B.S.; Novikova, L.I.; Frankevich, E.L. Photogeneration of Current Carriers in Crystalline Tetracene in a Magnetic Field. *J. Exp. Theor. Phys.* **1970**, *31*, 842-845.

7. Bree, A.; Lyons, L.E. 1002. The Intensity of Ultraviolet-Light Absorption by Monocrystals. Part IV. Absorption by Naphthacene of Plane-Polarized Light. *J. Chem. Soc. (Resumed)*, **1960**, 0, 5206-5212.
8. Wilson, M. W. B.; Rao, A.; Johnson, K.; Gélinas, S.; di Pietro, R.; Clark, J.; Friend, R. H. Temperature-Independent Singlet Exciton Fission in Tetracene. *J. Am. Chem. Soc.* **2013**, *135*, 16680-16688.
9. Wagemans, W.; Janssen, P.; Schellekens, A. J.; Bloom, F. L.; Bobbert, P. A.; Koopmans, B. The Many Faces of Organic Magnetoresistance. *SPIN* **2011**, *01*, 93-108.
10. Jang, H.-J.; Pookpanratana, S. J.; Brigeman, A. N.; Kline, R. J.; Basham, J. I.; Gundlach, D. J.; Hacker, C. A.; Kirillov, O. A.; Jurchescu, O. D.; Richter, C. A. Interface Engineering to Control Magnetic Field Effects of Organic-Based Devices by Using a Molecular Self-Assembled Monolayer. *ACS Nano* **2014**, *8*, 7192-7201.
11. Bittle, E.G.; Biacchi, A.J.; Fredin, L.A.; Herzing, A.; Allison, T.C.; Hight Walker, A.R.; Gundlach, D.J. Correlating Anisotropic Mobility and Intermolecular Phonons in Organic Semiconductors to Investigate Transient Localization. *Accepted to Comm. Physics*.
12. Tavazzi, S.; Raimondo, L.; Silvestri, L.; Spearman, P.; Camposeo, A.; Polo, M.; Pisignano, D. Dielectric Tensor of Tetracene Single Crystals: The Effect of Anisotropy on Polarized Absorption and Emission Spectra. *J. Chem. Phys.* **2008**, *128*, 154709.